UNIVERSITAT POLITÈCNICA DE VALÈNCIA

ETSI Aeroespacial y Diseño Industrial

UNIVERSITAT POLITÈCNICA DE VALÈNCIA

School of Aerospace Engineering and Industrial Design

Computational aerodynamic characterization of an UAV during cruise and take-off conditions

Master's Thesis

Master's Degree in Aeronautical Engineering

AUTHOR: Vandewalle, Tibo

Tutor: Quintero Igeño, Pedro Manuel

ACADEMIC YEAR: 2023/2024

Clean Mobility & Thermofluids

UNIVERSITAT POLITÈCNICA DE VALÈNCIA

Master thesis

Computational aerodynamic characterization of an UAV during cruise and take-off conditions.

Student:	Tibo Vandewalle – tvandew@etsid.upv.es
Student number:	r0843965 (home university) – P021203331 (host university)
Supervisor (home university):	Derdaele, Johan – johan.derdaela@kuleuven.be
Supervisor (host university):	Quintero Igeño, Pedro Manuel – pedquiig@mot.upv.es

Academic year: 2023-2024

1 NOMENCLATURE

$C_{P_{air}}$	specific heat of air
M_{air}	molar mass of air
μ_{air}	viscosity of air
P_{atm}	atmospheric pressure
T_{inf}	freestream temperature
R_{gas}	ideal gas constant
R_{air}	gas constant
γ_{air}	heat capacity ratio
a_{inf}	speed of sound
M_{inf}	freestream Mach number
v_{inf}	freestream velocity
ρ_{air}	density of air
L	lift
C_L	lift coefficient
D	drag
C_D	drag coefficient
S	airfoil surface
q_{inf}	dynamic pressure
T	thrust
C_T	thrust coefficient
Q	torque
C_Q	torque coefficient
P	power
C_P	power coefficient
J	advance ratio
Jn	normal advance ratio
η	efficiency
β	freestream angle
n	rotational speed
ω	rotational speed

θ	radial position
d	propeller diameter
R	propeller radius
r	propeller section distance

2 Contents

3 INTRODUCTION

The study of unmanned aerial vehicles (UAVs) has gained significant attention due to their expanding applications in both civilian and military sectors. The aerodynamic performance of UAVs, especially during cruise and take-off conditions, is critical to their overall efficiency and effectiveness. This master's thesis focuses on the computational aerodynamic characterization of a UAV's propeller, providing a comprehensive analysis of its behavior in various flight conditions using advanced computational methods. This research builds upon the work of Brendan Mullen (2024), who conducted a master's thesis on the same UAV but focused on vertical flight dynamics.

While there is an abundance of literature on vertical flight analyses, there is a noticeable scarcity of studies examining the computational fluid dynamics (CFD) of propellers in horizontal flight. Addressing this gap, the primary goal of this research is to enhance the understanding of the aerodynamic properties of UAV propellers in horizontal flight through CFD simulations. STAR-CCM+, a CFD software, is employed to model and simulate propeller performance. However any other CFD software can be used.

This study investigates key aerodynamic parameters such as lift, drag, thrust, torque, and propeller efficiency, providing detailed insights into the propeller's behavior under various flight conditions. The methodology section outlines the different simulation techniques used, including the Blade Element Method (BEM), Moving Reference Frame (MRF), and Rigid Body Motion (RBM). These methods are applied to model the propeller's interaction with the surrounding air, allowing for a thorough analysis of the UAV's performance in diverse flight scenarios.

The simulation results are compared with theoretical models and experimental data to validate the findings. Additionally, the study explores the effects of various parameters, such as advance ratio, freestream angle, and rotational speed, on propeller performance. This comprehensive approach aims to provide a deeper understanding of the aerodynamic characteristics of UAV propellers, contributing to the optimization and advancement of UAV design and performance.

4 METHODOLOGY

4.1 CFD

Computational Fluid Dynamics (CFD) is a powerful computational tool used to analyze and simulate the behavior of fluids and their interactions with solid surfaces. It has broad applications across many industries, including aerospace, automotive, energy, and environmental engineering. The fundamental principles of CFD are rooted in the mathematical formulation and numerical solutions of fluid flow, which are governed by the Navier-Stokes equations.

The core of CFD is the Navier-Stokes equations, which describe the motion of viscous fluid substances. These equations are derived from the principles of conservation of mass, momentum, and energy.

- Conservation of Mass (Continuity Equation):

$$\frac{\partial \rho}{\partial t} + \nabla \cdot (\rho u) = 0$$

This equation ensures that mass is conserved in the fluid flow, where ρ is the fluid density and u is the velocity field.

- Conservation of Momentum (Navier-Stokes Equations):

$$\rho\left(\frac{\partial u}{\partial t} + u \cdot \nabla u\right) = -\nabla p + \mu \nabla^2 u + f$$

These equations describe the change in momentum of fluid particles, where p is the pressure, μ is the dynamic viscosity, and f represents body forces such as gravity.

- Conservation of Energy:

$$\rho\left(\frac{\partial E}{\partial t} + u \cdot \nabla E\right) = -\nabla \cdot \mathrm{q} + \Phi$$

This equation accounts for the energy transfer within the fluid, where E is the total energy, q is the heat flux, and Φ is the dissipation function.

To solve the Navier-Stokes equations, the continuous fluid domain is discretized into a finite set of control volumes or computational cells. This process transforms the partial differential equations (PDEs) into algebraic equations that can be solved numerically (Ansys, 2024).

4.2 Propeller and drone

The propeller discussed in this paper is the MS1101 propeller from T-motor. This propeller is used on the Hunter mini UAV. The table below shows the specifications of the propeller as provided by the manufacturer.

Figure 1: MS1101 propeller

Table 1: MS1101 specifications

Model	**MS1101**
Weight	10g
Diameter	280,3mm
Pitch	106,68mm
Thrust at 4700rpm	400g
Thrust at 7100rpm	900g
Thrust at 11000rpm	2000g

Using a 3D-scanner a cad-file is made so the propeller can be analyzed in the CFD software (*T-MOTOR Official Store*, z.d.).

4.3 Aerodynamic parameters

To understand the conclusions made in the paper, the two basic parameters, lift and drag need to be understanded. In the BEM analyze, the airfoil sections will be simulated to retrieve these two parameters for different situations.

When an object, in this case an airfoil is placed in a moving fluid, two force distributions are developed around the profile, this is the pressure distribution and the shear stress distribution. The pressure vectors are perpendicular to the surface and the shear stress vectors are tangential to the surface (Fraser-Mitchell, 2012b).

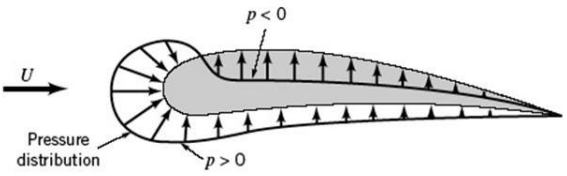

Figure 2: Pressure distribution

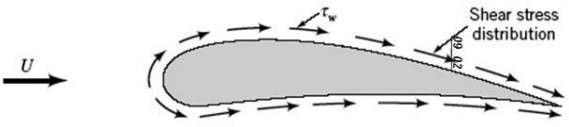

Figure 3: Shear stress distribution

The sum of the two force distributions results in a single force. When this force is broken down, it has two components: one horizontal and one vertical. These components are called drag and lift, respectively.

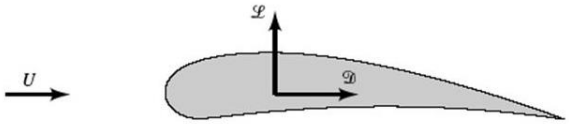

Figure 4: Resulting forces (Flow Over Immersed Bodies, 2017)

Out of those two forces, the corresponding coefficients can be determined:

$$C_L = \frac{L}{q_{inf} \cdot S}$$

$$C_D = \frac{D}{q_{inf} \cdot S}$$

With the dynamic pressure equal to:

$$q_{inf} = \frac{1}{2} \cdot \rho_{inf} \cdot {v_{inf}}^2$$

Advance ratio

The advance ratio, denoted as J, is a dimensionless parameter that characterizes the performance of a propeller. It provides a measure of the relationship between the freestream velocity and the rotational speed of its propeller. The advance ratio is defined by the following equation:

$$J = \frac{v}{n \cdot d}$$

The advance ratio quantifies how far the vehicle travels forward during one complete rotation of the propeller, normalized by the diameter of the propeller (Day, 2000).

Propeller thrust

Thrust is the force generated by a propeller that propels an aircraft through a fluid. In the context of a propeller, thrust is the resultant force in the direction of the propeller axis.

The thrust coefficient is a dimensionless parameter that characterizes the thrust of a propeller. It relates the thrust generated by the propeller to the fluid density, rotational speed, and diameter of the propeller. The formula for thrust coefficient is (Day, 2000):

$$C_T = \frac{T}{\rho \cdot n^2 \cdot d^4}$$

Propeller torque

The propeller torque is the resulting moment, with respect to the propeller axis, of all the forces that are exerted on the propeller. The coefficient related to this propeller torque is defined as (Day, 2000):

$$C_Q = \frac{Q}{\rho \cdot n^2 \cdot d^5}$$

Propeller power

Power in the context of a propeller is the rate at which energy is transferred to the fluid through the rotation of the propeller. It is directly related to the thrust and drag forces.

The power coefficient is a dimensionless parameter that relates the mechanical power output of the propeller to the power input. It is defined as (Day, 2000):

$$C_P = \frac{P}{\rho \cdot n^3 \cdot d^5}$$

Propeller efficiency

P is the power needed to make the propeller spin at the desired speed. The power available for propulsion is the thrust multiplied by the velocity. Therefore, propeller efficiency is the ratio of the power produced (output) to the power supplied (input).

$$\eta = \frac{v_{inf}}{n \cdot d} \cdot \frac{C_T}{C_P}$$

A typical propeller characteristics plot is shown below to compare later to the results obtained by the CFD simulations. All the parameters explained above come together in this single plot (Day, 2000).

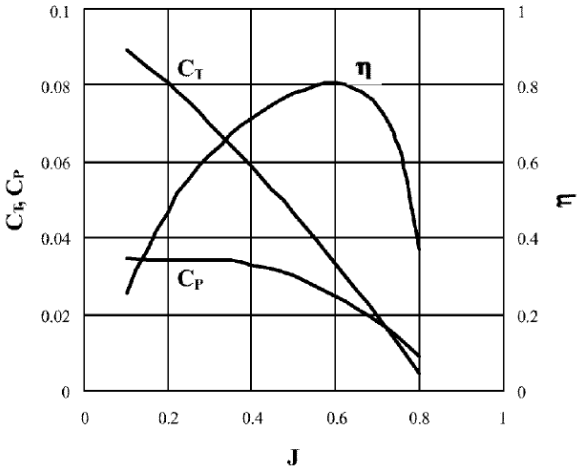

Figure 5: Typical propeller characteristics

The plot clearly shows that the thrust coefficient and power coefficient are highest at hover, corresponding to J = 0. However, efficiency is lowest in this scenario. As the advance ratio increases, both coefficients gradually decrease until they reach zero. Interestingly, efficiency initially increases slowly to its peak before sharply declining to zero. These observations will be compared with the simulations results, further in the report.

4.4 Goniometry/situation

To understand the analyses made in the next chapters, conventions are made regarding the angles used in the simulations and calculations.

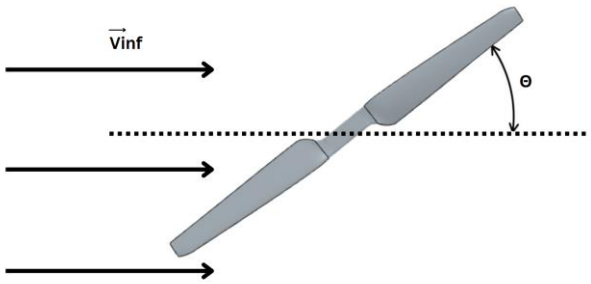

Figure 6: Front view situation

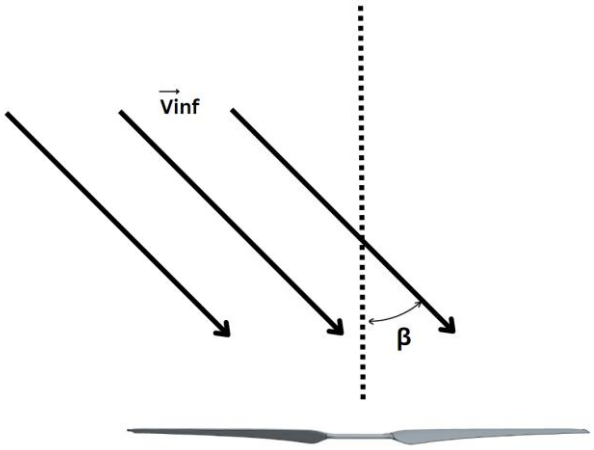

Figure 7: Top view situation

Analyzes are made are made for a variety of different parameters, two of which are the radial position and the freestream angle. The radial position represented by the Greek letter theta (θ) is the angle between the transverse length of the propeller and the positive x-axis, this value ranges from 0° to 360°, this when the propeller rotates counter clockwise according to figure 6 shown above.

The freestream angle represented by the Greek letter beta (β) is the angle between the freestream velocity vectors and the rotation axis of the propeller, represented in figure 7. The value for beta will range from 0° to 90°, where 0° represents pure vertical flight/flow and 90° pure horizontal flight/flow.

The simulations happen in ideal circumstances. Therefore the fluid parameters are selected, needed for the physics in the model.

Table 2: Fluid parameters

Parameter	Value
$C_{P_{air}}$	$1003{,}62 J/kg \cdot K$
M_{air}	$28{,}9664\ kg/kmol$
μ_{air}	$1{,}85508E-5\ Pa \cdot s$
P_{atm}	$101325{,}0\ Pa$
T_{inf}	$300K$
R_{gas}	$8314{,}5\ J/K \cdot kmol$

Using the parameters shown above, the following parameters can be obtained (Fraser-Mitchell, 2012).

$$R_{air} = \frac{R_{gas}}{M_{air}}$$

$$\gamma_{air} = \frac{C_{P_{air}}}{C_{P_{air}} - R_{gas}}$$

$$a_{inf} = \sqrt{\gamma_{air} \cdot R_{air} \cdot T_{inf}}$$

$$v_{inf} = J \cdot n \cdot d$$

$$M_{inf} = \frac{v_{inf}}{a_{inf}}$$

$$\rho_{air} = \frac{P_{atm}}{R_{air}} \cdot T_{inf}$$

Additionally the model is selected to the 'K-Omega Turbulence' model due to the wide range of applications, reliability and numerical stability (Bardina et al., 1997).

4.5 Simulation models

4.5.1 Virtual disk and BEM

The virtual disk model is based upon the principle of representing the propeller as an actuator disk to reduce the computational cost compared to MRF model. For the virtual disk model, different methods can be implemented, such as

- Body Force Propeller Method
- Blade Element Method
- 1D Momentum Method
- User Defined Method

Where the second one will be used further in this work.

The blade element method lays the groundwork for the virtual disk method. The BEM models the spinning propeller as a distribution of momentum sources. The strength of these sources and their variations are determined interactively based on the propeller's geometry and the local velocity field (Simcenter STAR-CCM+ CFD Software, n.d.).

So the blade geometry is not explicitly resolved, it must be specified in terms of chord and twist variations along the rotor radius that are plotted below.

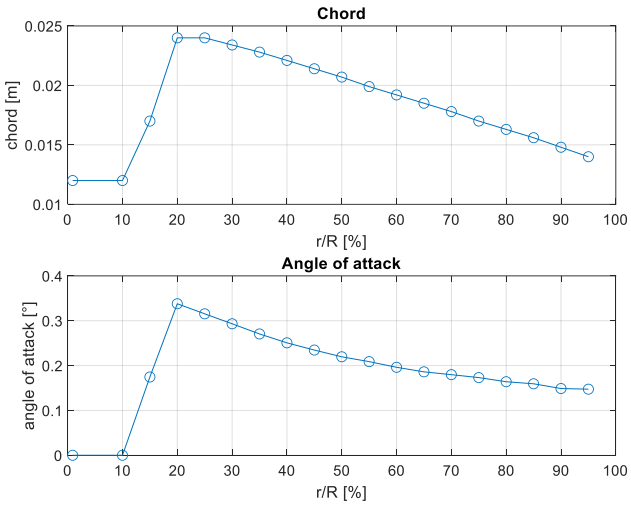

Figure 1: Chord and AoA in function of the radius

The lift and drag coefficient for two-dimensional cross-sections of the blade need to be simulated. These two parameters are studied across a range of angles of attack from -15 to +40 degrees, and at various Reynolds numbers, including (1000, 2000, 4000, … 128000, 150000).

The sections are taken where the profile of the propeller changes the most. This contains both the hub and the blades itself.

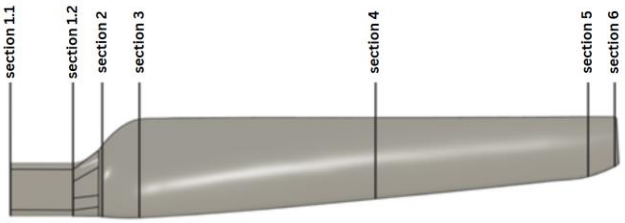

Figure 2: Blade sections visualization

As shown in the picture above, the sections 1-6 are taken at 0%, 10%, 15%, 21%, 60%, 95% and 99% respectively. Where the sections 0% and 10% are identical and are representing the hub.

For each section the dimensions are analyzed, mainly the chord and the AOA (α). These parameters are used later in the BEM. In the table below, the parameters are shown, the third column is the same as the second column but slightly rounded.

Table 1: Section parameters

Section	r [m]	r/R [ ]	r'/R [%]	chord [m]	angle [°]
1 (hub)	0,00	0,00	0,00	0,0125	0,00
2 (hub)	0,0144	0,103	10,3	0,0125	0,00
3	0,0210	0,157	15,0	0,0167	10,0
4	0,0296	0,211	21,1	0,0242	18,9
5	0,084	0,579	60,0	0,0197	11,0
6	0,133	0,946	95,0	0,0140	8,01
7	0,139	0,994	99,0	0,0115	7,98

Each section has a different geometry, therefore different meshes for the boundary layers are used for each section, but the same meshes for the fluid domain.

The boundary layer thickness changes in function of the Reynolds, more, in function of the rotational speed. This last one will vary from 4700rpm up to 11000rpm. We want to make sure that for each rotational speed, the boundary layer is simulated appropriately, therefore the mesh is setuhp for the biggest boundary layer. This situation will occur at a rotational speed of 4700rpm, this because the Reynolds is proportionate to the rotational speed.

Table 2: Boundary layer estimation, 4700rpm

n=4700rpm; μ=1,86E-5 N·s/m²			
section	r · ω [m/s]	Re [ ]	estimated δ99 [m]
1 (hub)	0,00	0,00E+00	/
2 (hub)	7,09	5,63E+03	6,95E-04
3	10,3	1,10E+04	6,66E-04
4	14,6	2,25E+04	6,75E-04
5	41,3	5,20E+04	3,62E-04
6	65,5	5,86E+04	2,43E-04

To verify that the boundary layers are the biggest at a rotational speed of 4700rpm, the estimated δ99 is also calculated for a rotational speed of 11000rpm.

Table 3: Boundary layer estimation, 11000rpm

n=11000rpm; μ=1,86E-5N·s/m²			
section	r · ω [m/s]	Re [ ]	estimated δ99 [m]
1 (hub)	0,00	0,00E+00	/
2 (hub)	16,6	1,32E+04	4,54E-04
3	24,2	2,57E+04	4,35E-04
4	34,1	5,26E+04	4,41E-04
5	96,8	1,22E+05	2,37E-04
6	153	1,37E+05	1,59E-04

4.5.2 MRF

The Moving Reference Frame (MRF) model is a steady-state approach used to simulate the behavior of a propeller using its CAD model. This model requires two distinct regions: a rotating domain and a static domain. The rotating domain, which contains the CAD model of the propeller, rotates at the desired speed around the body's axes while the body remains stationary, while the static domain and the propeller remains stationary. The rotating domain is typically dimensioned as a cylinder with a height of 0,7 times the diameter of the propeller and a diameter of 1,5 times the diameter of the propeller (Yu et al., 2023).

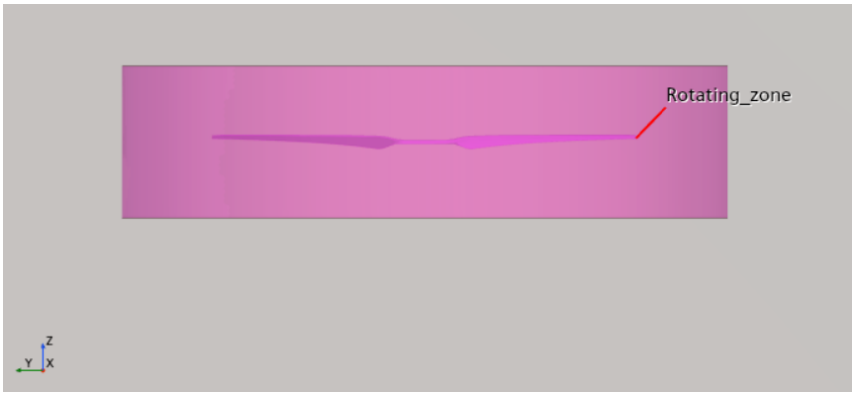

Figure 3: Rotating domain

When handling with oblique flow, the orientation of the propeller can't be neglected. When the propeller is rotated 90° degrees, the velocities are different when compared to the previous position of 0°. As illustrated in the figures below, the blades will experience different velocities. For example at figure 11 where the blades are horizontal, the velocities at both blades will be equal. However at figure 12 where the blade is rotated 90°, the approaching blade of the propeller will experience a higher velocity than the opposite (retreating) blade. This with the assumption the rotational movement of the blade does not impact the incoming flow drastically.

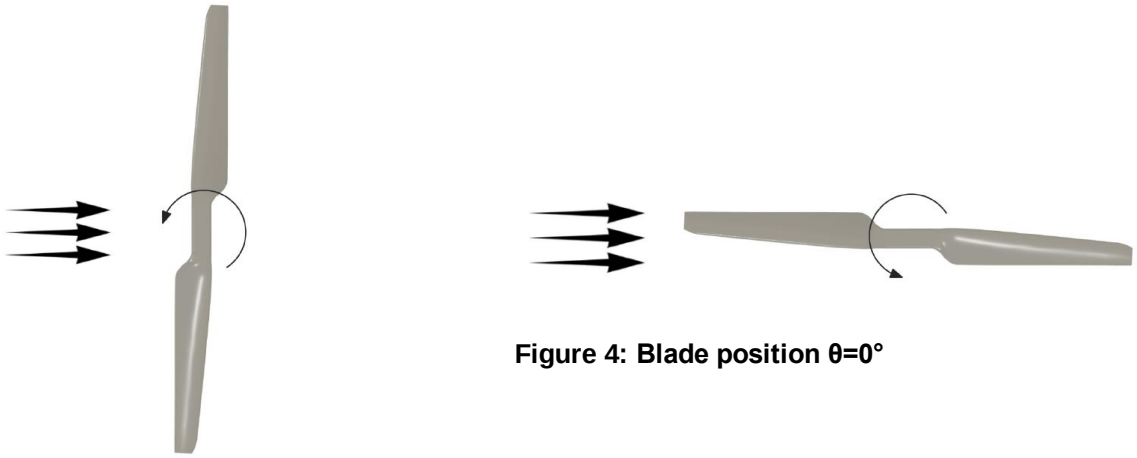

Figure 4: Blade position θ=0°

Figure 5: Blade position θ=90°

In basic aerodynamics, lift increases as the flow speed increases. Also when the advancing blade has a higher horizontal speed, so its angle of attack rises, resulting in higher lift. This happens even though the vertical freestream speed stays the same. The picture below shows this: on the left, the airfoil represents the advancing blade, and on the right, it represents the retreating blade. You can see that with the same vertical speed, an increase in horizontal speed, increases the angle of attack.

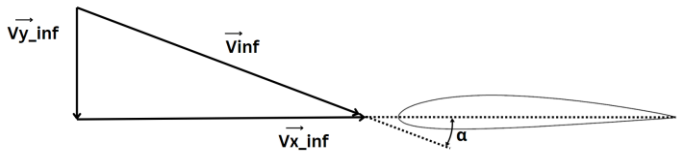

Figure 6: Illustration advancing blade

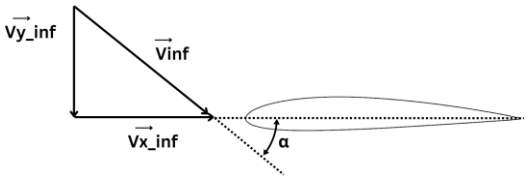

Figure 7: Illustration retreating blade

Assuming this theory, the simulation should show a difference in thrust between the two blades, with the advancing blade generating more thrust than the retreating blade.

As mentioned before, the rotating region and the static region are two different geometries, however there has to be an interaction between the two. This can be realized by an interface for each face of the common faces, in this case are the faces the top, bottom and the side of the rotating region. The type of interface can be important depending on what we need to analyze.

Primary there are two types of interfaces analyzed, the mixing-plane interface and the internal interface. The mixing-plane interface is the most basic of the two, it can be used when we are not interested in the influence of the radial position of the blade. This because the mixing-plane interface takes the average so that the force distribution along the blade is pure symmetrical. This can by handy when handled with normal airflow or airflow with an advance ratio equal to zero. The internal interface by the other hand can be used to analyze the difference in behavior of each blade.

4.5.3 RBM

To analyze what's really happening around the blade surface, a transient simulation is implemented to hopefully solve the MRF problem. A transient simulation is applied, also known as RBM (=Rigid Body Motion). It involves actual rotation of the propeller geometry. This should result in a more realistic physic response. Of course this is way more numerically complicated and computationally expensive than the MRF. Therefore the following simulations were done on the cluster provided by CMT (Johan, 2022).

The RBM simulations uses the same geometry, domain and mesh setup at the MRF simulations. As it comes to the RBM parameters, the propeller moves in steps of five degrees with a rate of 4700rpm.

$$stepsize = 5°$$

$$timestep = stepsize \cdot \frac{\pi}{180° \cdot \omega}$$

$$= 5° \cdot \frac{\pi}{180° \cdot \frac{4700rpm \cdot 2 \cdot \pi}{60}} = 1{,}776E-4s$$

$$time\ for\ one\ rotation = \frac{360°}{stepsize} \cdot timestep = 0{,}0128s$$

The simulation is run for three different advance ratios: 0.2, 0.4, and 0.8. For each advance ratio, the propeller turns twenty times to make sure the results are stable. So, for one angle of oblique flow, the total simulation involves 60 propeller rotations.

4.6 Simulation operations

The model that is set up needs to be simulated for a lot of different situations takes a lot of time. Simulation operations are a tool to make simulating these easy. It goes trough a cycle that can changes parameters whenever needed, for example when the situation converged. This tool is used on the BEM, VD, MRF and on the RBM

The BEM model is simulated for 55 different degrees and 9 different Reynolds numbers who will result in different freestream velocities. This means that each section of the propeller needs to be simulated for 495 situations.

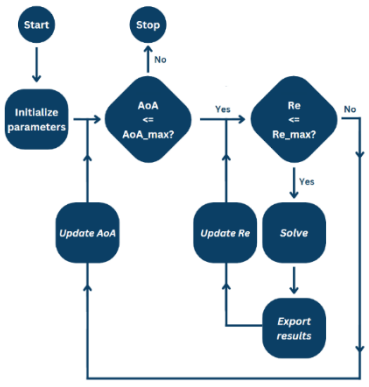

Figure 8: Simulation operation BEM

The same counts for the VD and MRF where the advance ratio and the angle beta is adapted, the advance ratio from 0 to 0.8 and the angle from 0 to 90 degrees.

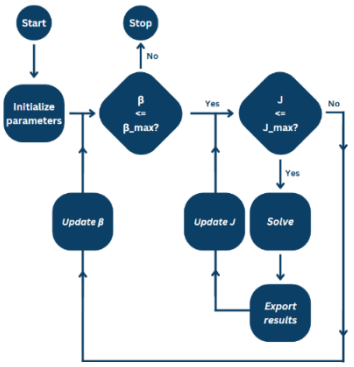

Figure 9: Simulation operation VD and MRF

Finally, the RBM takes a different approach. Instead of adjusting the angle, only the advance ratio is modified. This decision is made to avoid wasting time if error will occur, this because the simulation is ran on a server without the ability to monitor it.

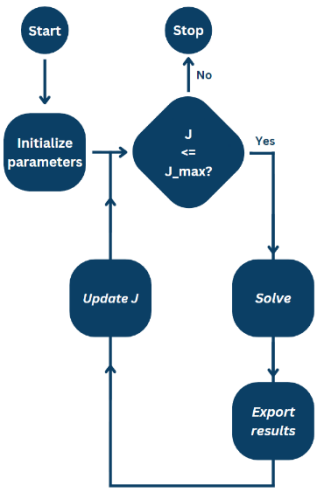

Figure 10: Simulation operation RBM

4.7 Regions and domain validity

The domain for the 2D simulations for the BEM consists of three regions: the inlet, the outlet, upper/lower wall and the airfoil. Those three regions are respectively defined as a velocity inlet, pressure outlet, slip wall and no-slip wall.

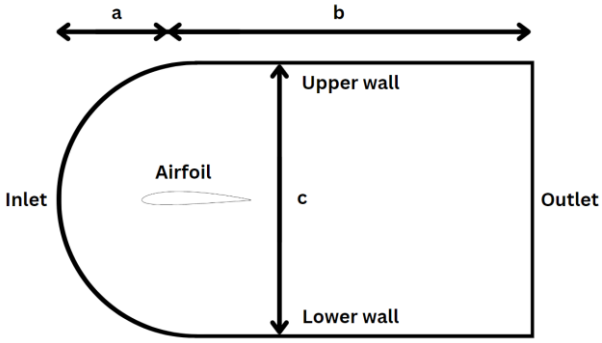

Figure 11: BEM domain size

The domain size is setup for the biggest airfoil section. This is the fourth section with a chord of 0,0242m. Therefore a principle will be used where the size of the domain will be adapted so the difference in velocity along the region (upper/lower wall and outlet) compared to the reference velocity (vinf) should be as low as possible, around 5% (Bekaert, z.d.). This method will happen with the finest mesh used in the mesh comparison that is shown further in the paper.

$$\%error_{v_{max}} = \frac{|v_{inf} - v_{max}|}{v_{inf}} \cdot 100\% \leq 5\%$$

$$\%error_{v_{min}} = \frac{|v_{inf} - v_{min}|}{v_{inf}} \cdot 100\% \leq 5\%$$

A domain with the dimensions where a and c/2 is equal to ten times the chord and b equal to twenty times the chord seems a good size choice.

Table 4: Domain dimensions

Parameter	Size
a	5 · chord
b	20 · chord
c	10 · chord

For both regions, the dimensions shown above were determined for the most extreme conditions, this means for the inlet the condition where Re = 150 000 and AoA = 40°. To determine the distance of the outlet, a Re = 150 000 and AoA = 0° is used. This means that both situations will be examined at a freestream velocity (v_{inf}) of 97,3m/s.

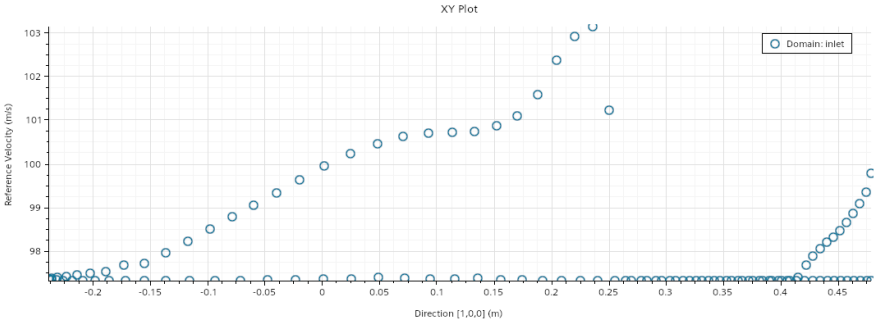

Figure 12: Velocity along the upper/lower wall

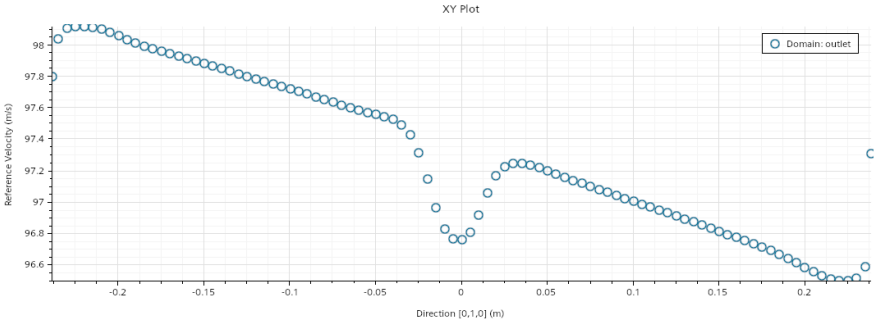

Figure 13: Velocity along the outlet

Table 5: Velocity analyze

	v_{max} [m/s]	v_{min} [m/s]	$error_{v_{max}}$ [%]	$error_{v_{min}}$ [%]
Inlet	103	94,3	**5,86**	0,00
outlet	98,1	96,5	**0,835**	0,831

The dimensions for the domain of the virtual disk, the MRF and the RBM are the same. Due to the study of oblique flow, the wake of the propeller will change in direction. Therefore a spherical domain is chosen with a relatively large radius of 8 meter is used. For the MRF, and additional domain is dimensioned, the rotating domain shown on the figure below. The same domain is valid for the virtual disk and the RBM except for the virtual disk, the static region is the only region present.

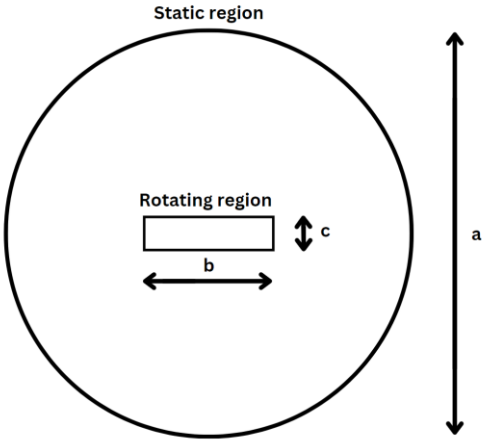

Figure 14: Domain regions

As it comes to the regions, the following region definitions are used:

Region	**Definition**
Static region (VD, MRF and RBM)	Freestream velocity
Propeller (MRF and RBM)	No-slip wall

The static region is represented as a freestream. In this region, the flow magnitude and direction are specified within the model. The flow magnitude is given by the Mach number

$$M_{inf} = \frac{v_{inf}}{\sqrt{\gamma_{inf} \cdot R_{inf} \cdot T_{inf}}}$$ (Fraser-Mitchell, 2012),

where the velocity depends on the advance ratio,

$$v_{inf} = J \cdot n \cdot d$$ (Fraser-Mitchell, 2012).

The flow direction is determined using the sine and cosine of the flow angle.

4.8 Mesh validity

4.8.1 BEM

To find an appropriate mesh for the fluid domain, trial and error is used. The number of elements is increased by reducing the mesh size. This number of elements in function of the lift coefficient is used determine a mesh size.

Because the hub section is a symmetrical profile, the theoretical coefficient for the lift is known (equal to zero) at an angle of attack of zero degrees.

Table 6: Different meshes

mesh	Minimum cell size [mm]	Wake [% of base]
1	1,00	5,00
2	0,500	5,00
3	0,100	5,00

The above parameters are used to determine the appropriate mesh. Extra to these parameters, a slow growth rate is used to have a slow transition from the minimum cell size to the base size of 100mm. The wake-refinement has a spread angle of +-25 degrees to simulate the wake of the airfoil for each value of angle of attack.

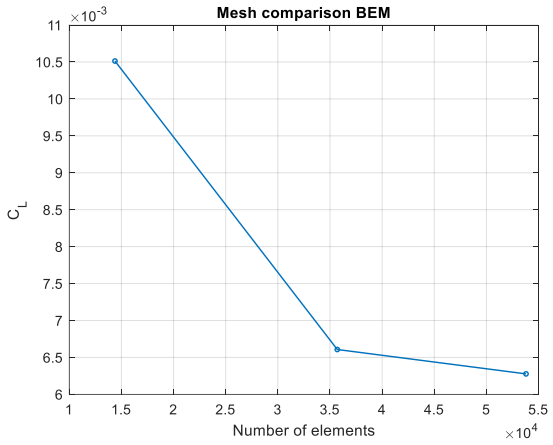

Figure 15: Mesh comparison BEM

The above plots shows that the use of a smaller wake than 5% does not affect the results with a great magnitude, this only effects the computational cost. Reducing the mesh around the profile has a greater effect on the results for Cl. Because we want the lowest value for Cl at an angle of attack of zero degrees (theoretical it should be zero), mesh 4 will be used to continue the simulations regardless the small difference in results between mesh 3 and 4.

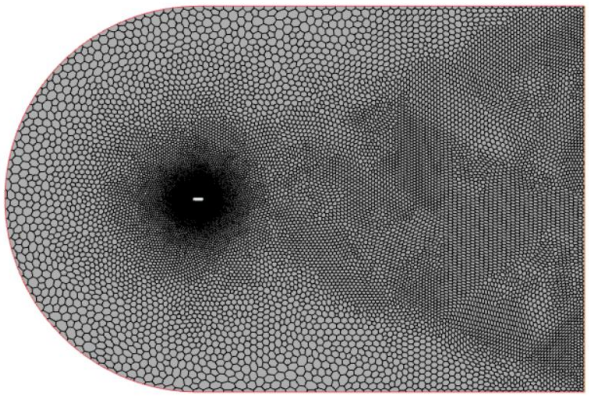

Figure 16: Mesh BEM

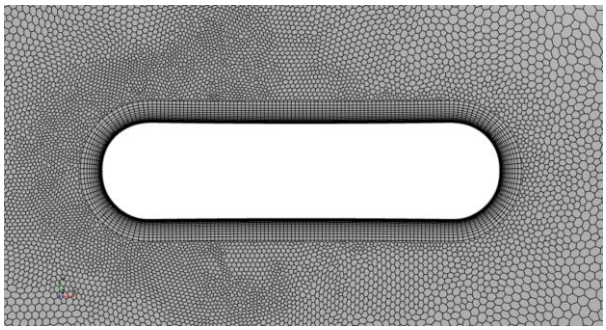

Figure 17: Prism layers BEM

As result, a mesh is created with the previously defined boundary layers, which the prism layers will obtain. As initial guess, twenty prism layers are used. To verify the quality of these prism layers, a y+ model is modelled. These y+ values must be below 5 or even below 1 would be better. The figure below verifies the correct prism layers.

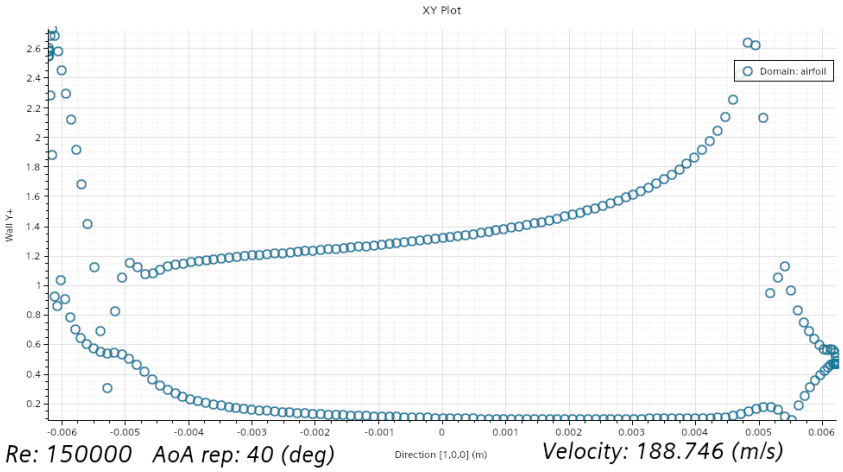

Figure 18: Y+ plot BEM

4.8.2 VD

Following the dimensioning of the domain, a correct mesh is chosen. Therefore four meshes are chosen where the responding thrust coefficient is plotted in function of number of elements. Analyzing the figure below, it's clear the third mesh is the most suitable mesh taking the number of elements in account. An asymmetrical wake is added to have a wake suitable for different values of beta. For the exactly, more detailed setup of the virtual disk I'd like to refer to the work of Brendan (Mullen, 2024)

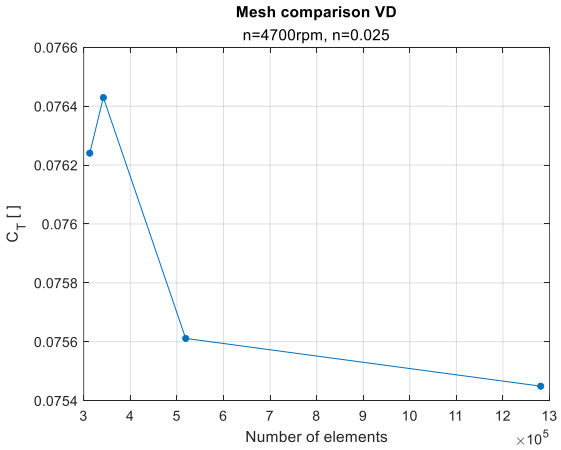

Figure 19: Mesh comparison VD

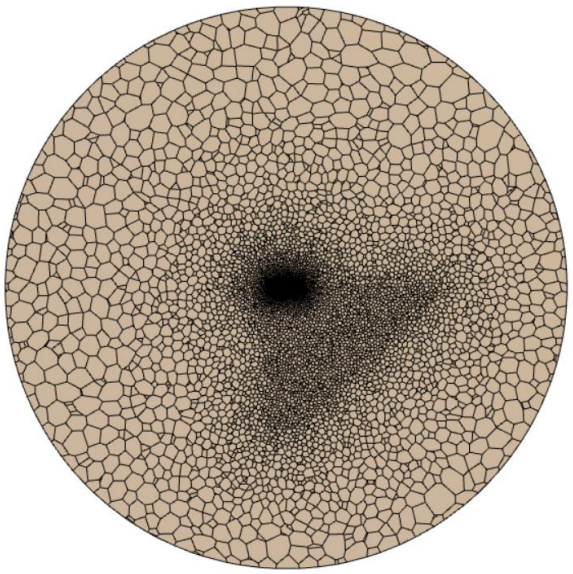

Figure 20: Mesh VD

4.8.3 MRF and RBM

Just like the virtual disk, a mesh is chosen. Taking into account the number of cells in relation to the computational cost, mesh 2, which contains 1.7 million cells, is chosen due to the small change of the thrust coefficient between the second and the third mesh but a huge difference in elements.

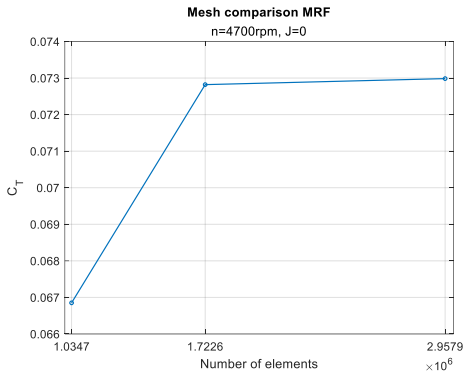

Figure 21: Mesh comparison MRF

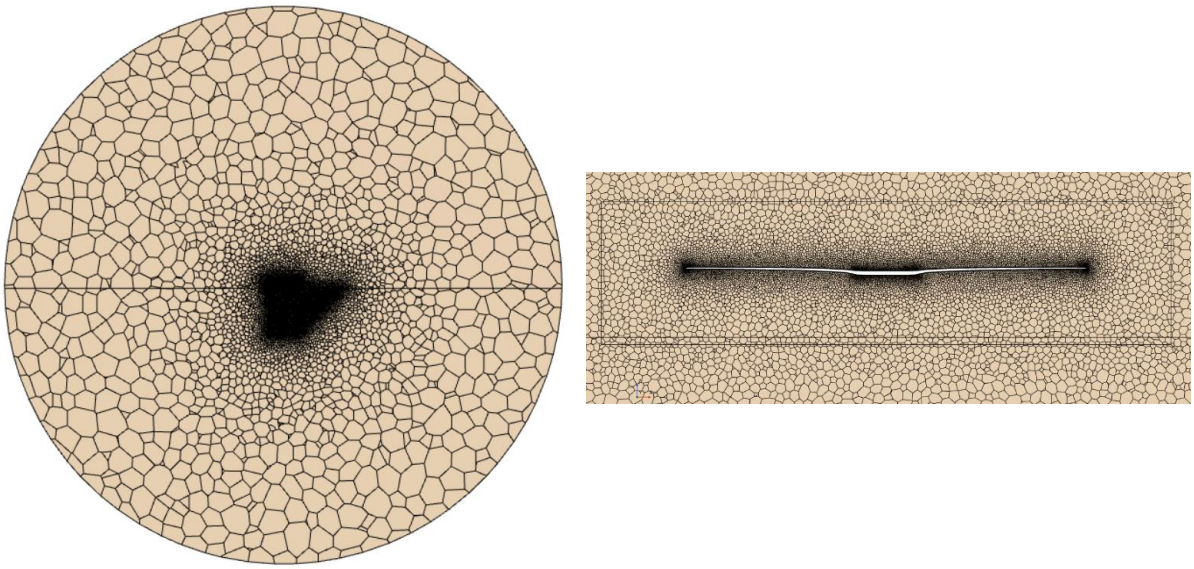

Figure 22: Mesh MRF and RBM

The wall+ plot of the propeller verifies that the prismatic layers around the propeller are valid.

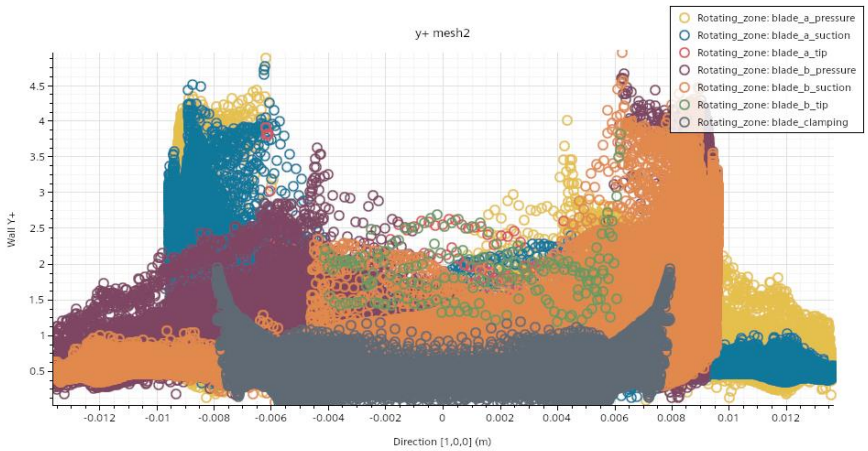

Figure 23: Y+ MRF and RBM

5 RESULTS

5.1 BEM

The results shown below are for section five of the propeller. Both the lift- and the drag coefficient needs to be imported in the virtual disk model in function of the angle of attack and the Reynolds number. The other results of the sections can be consulted in the attachments. The results of these plots are implemented in the form of tables in the virtual disk. All the plots have the same kind of behavior.

As example for section 6 a few observations can be made. As shown below the airfoil will enter stall at a certain point. The angle of attack where the stall happens, depend slightly on the Reynolds number. Only from Reynolds numbers of 16000 or higher, stall happens. The stall is noticeable on the figure below where the lift coefficient drops unexpected. The angle of attack for stall, rises in function of the Reynolds. This means, how higher the velocity (and thus higher the Reynolds number), how higher the maximum lift coefficient and how higher the angle of attack where stall happens.

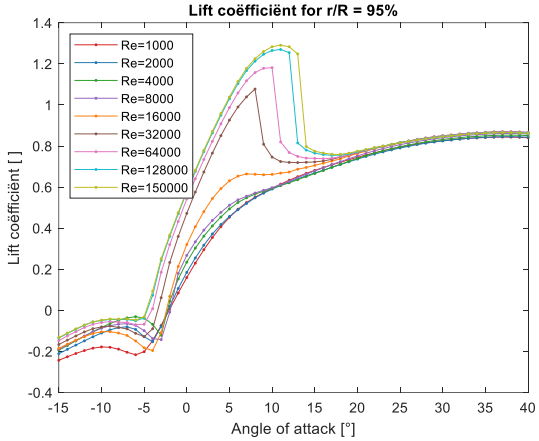

Figure 25: Results C_L section 6

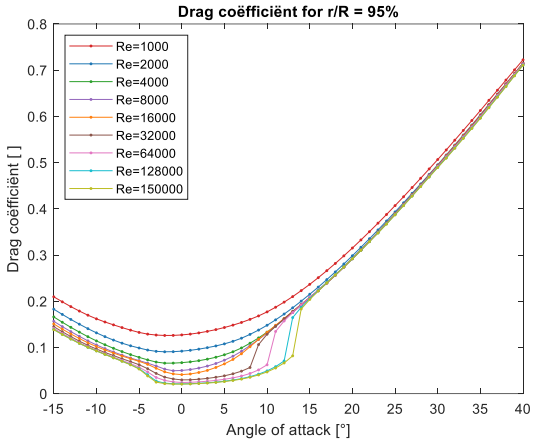

Figure 24: Results C_D section 6

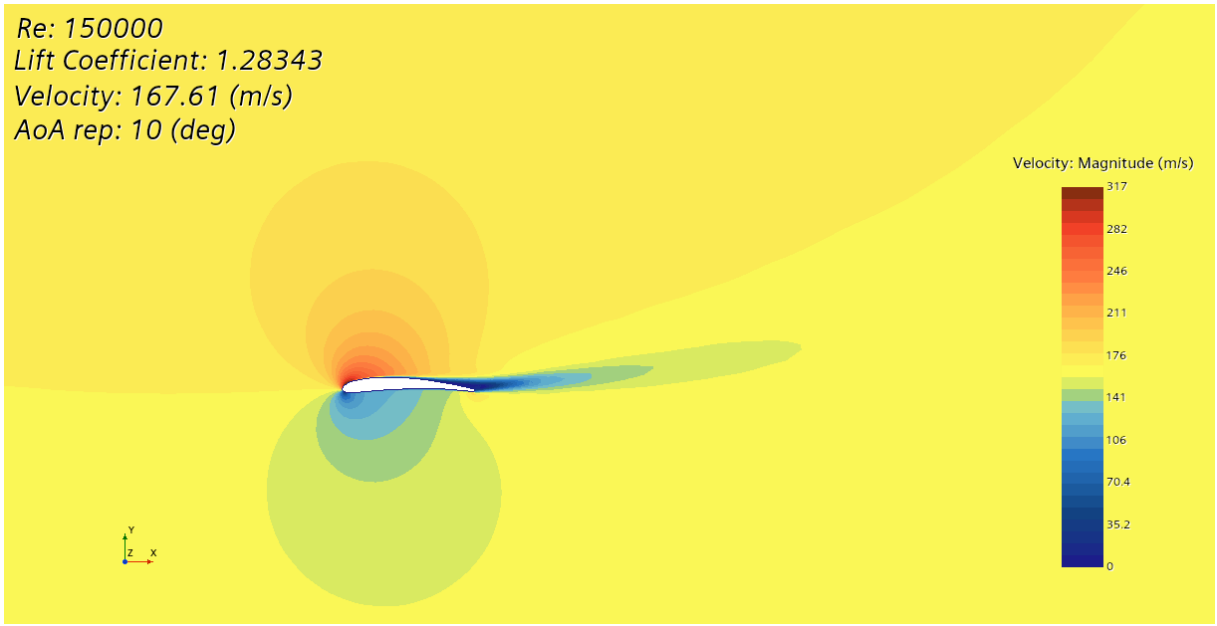

Figure 26: Velocity around airfoil, no stall

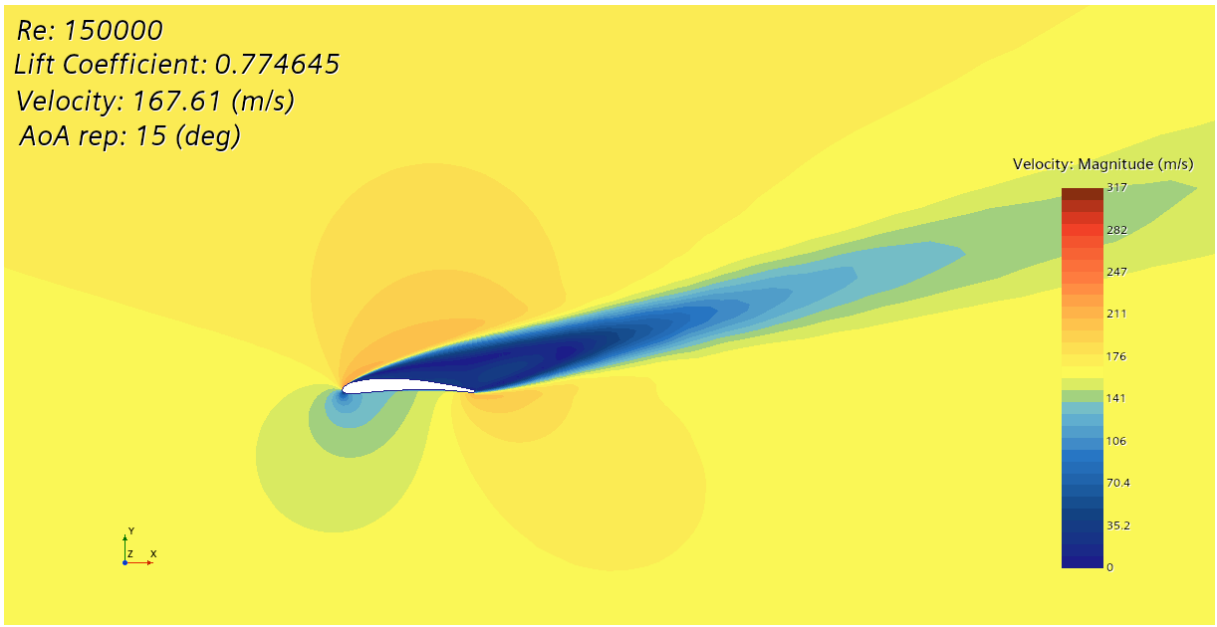

Figure 27: Velocity around airfoil, stall

5.2 Virtual disk

Primarily the virtual disk was executed with no sixth section. A sixth section with the purpose to simulate the tips of the propeller more accurate, this because the velocities at the ends of the blade are the highest. However, this does not seem to be a big deal. Shown in the plots below, there is only a minor difference off less than one percent at a rotational velocity of 4700rpm. The small difference can be explained due to the tip-loss effect at the tips on the blades, which makes the use of a sixth section at the tips not a gamechanger.

The "tip loss effect" is the reduction in aerodynamic efficiency and performance of a blade or wing due to the presence of tip losses. These losses occur at the blade tips and result in a decrease in the lift force generated by the blade, leading to lower overall energy capture. This phenomenon explains why the sixth section has a small impact on the results (Miao et al., 2022).

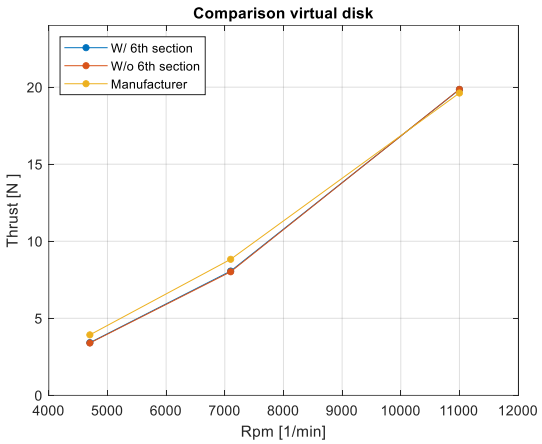

Figure 28: Comparison virtual disk

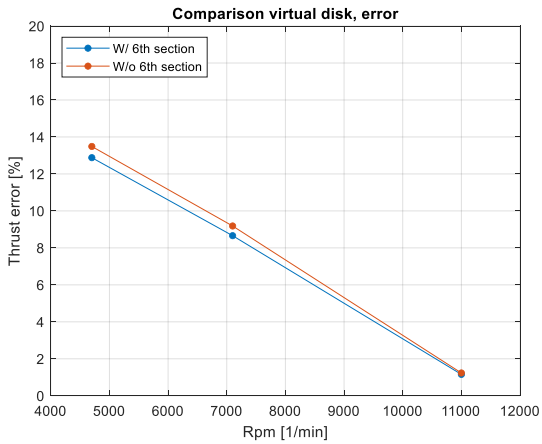

Figure 29: Comparison virtual disk, error

Table 7: Comparison virtual disk

n [rpm]	Thrust manufacturer [N]	Thrust w/ 6th section [N]	Thrust w/o 6th section [N]
4700	3,92	3,42	3,40
7100	8,83	8,06	8,02
11000	19,6	19,9	19,9

Compared to the manufacturer's data, the biggest difference in thrust is seen at a rotational speed of 4700 rpm. This error gets smaller as the speed goes up. There are two main reasons for this error could be: First, the mesh could be refined even more, but this would need more computational power, which is limited. Second, we don't know the exact test conditions the manufacturer used, like pressure, temperature and gas constants. For this analysis, we assume standard test conditions.

Propeller characteristics

A propeller is characterized by the propeller efficiency, thrust coefficient and power coefficient in function of the advance ratio. In this case, the characterization is done for two values for the rotational speed, 4700rpm and 11000rpm.

The small simulation operation is used to gather the necessary information efficiently. Data is taken for advance ratio jumps of 0,01, starting from 0,01. Due to this small difference of advance ratio, the simulation could think the task is converged directly after updating to the new advance ratio. Applying a minimum amount of iterations as a stopping criteria gives the program time to adapt to the small change of advance ratio so it can converge in the correct situation.

The results of the simulation shown below shows us a typical characterization plot for a propeller. It is clear that when the vertical velocity increases (thus the advance ratio increases), the thrust coefficient drops while the efficiency rises. This means that the in a hover position the propeller can produce the highest amount of thrust, this counts for every positive value of rotational speed.

When the rotational speed is increased, the max efficiency rises and thus the max thrust coefficient rises too.

This is according to the literature where for all propellers: With an increasing advance ratio, the propulsive efficiencies first increase slowly to the maximum values at a certain advance ratio. After this, the efficiency drops more quickly to zero. Just like the thrust coefficient, the power coefficient should decrease gradually to zero in function of the advance (Liu et al., 2016).

This is certainly not the case with the virtual disk, the power coefficient depends on the torque, this parameter is plotted in figure 32 in function of the advance ratio. It shows clearly that this parameter does not decrease gradually and does not converges to zero as citated in the literature.
This may be a sign that the virtual disk is not suitable for propeller characterization.
The virtual disk shows that the highest power is accomplished at an advance ratio of 0.14, this for an rpm of 4700 and 11000. The power coefficient decreases when the rotational speed decreases.

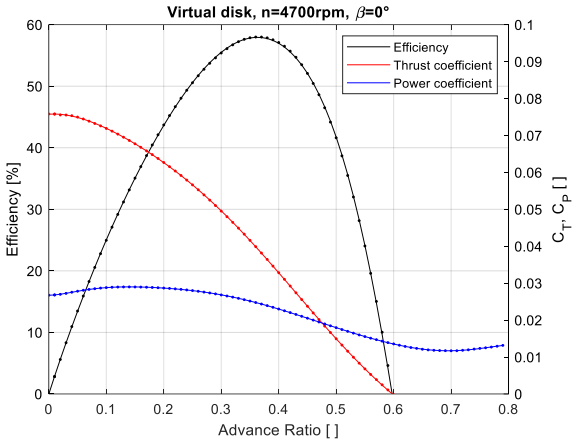

Figure 31: VD characteristics 4700rpm

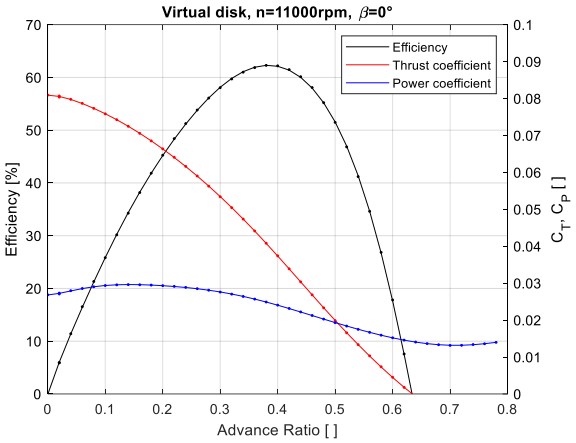

Figure 30: VD characteristics 11000rpm

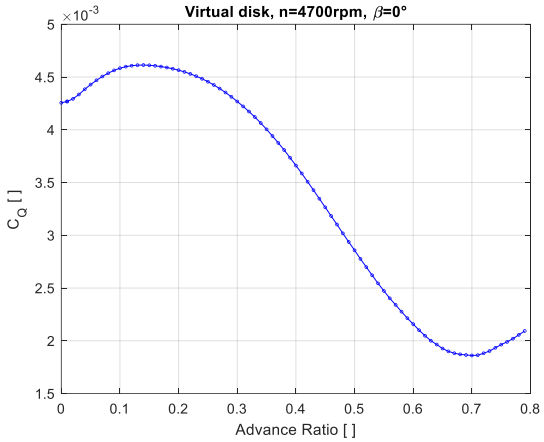

Figure 32: VD torque

5.2.1 Virtual disk in oblique flow

For the oblique flow, the same conventions regarding the angles are made, where beta is the angle of oblique flow, shown below.

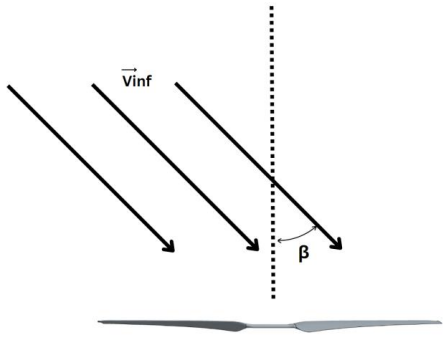

Figure 33: Angle beta, oblique flow

Following the characterization in perfectly perpendicular flow where the advance ratio is constantly equal to the normal advance ratio towards the propeller, the propeller as a virtual disk is analyzed in oblique flow.

Just like all the other simulations, a simulation operation is applied again. For different angles for β a characterization plot is made. The efficiency and the thrust coefficient are plotted in function of the advance ratio and for different values of β.

The plots below are showing a strange behavior when β is being increased. For β values greater than 40°, efficiency's higher than 100% are accomplished. Regarding the thrust coefficient, when a β of 60° is exceeded, the coefficient rises to infinity instead of decreasing to a value of zero. These strange behaviors are impossible and are completely counterintuitive according to the literature.

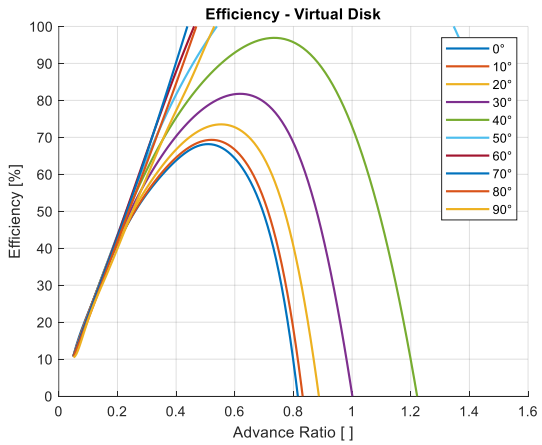

Figure 35: Efficiency VD in oblique flow

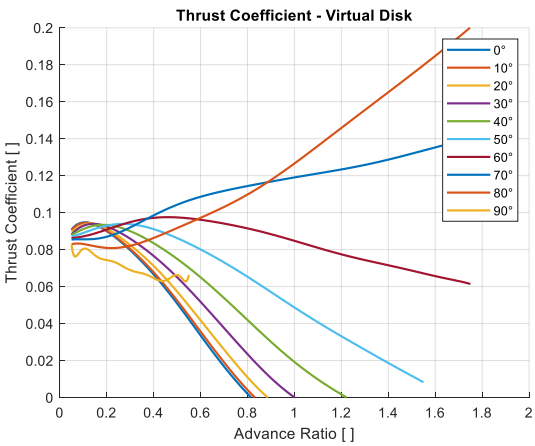

Figure 34: Thrust coefficient VD in oblique flow

Due to these results, further use of the virtual disk is required to be discontinued. The propeller will then be further analyzed using the MRF method, at the expense of increased computational costs.

5.3 MRF vertical flight

When comparing the result of the MRF with the data of the manufacturer, a bigger difference is found compared to the results of the Virtual disk. Just like the virtual disk, the percentual error drops in function of the rotational speed. A maximum error of a little over 15% is found at a rpm of 4700, and a minimum error of a small 4% at a rotational speed of 11000rpm.

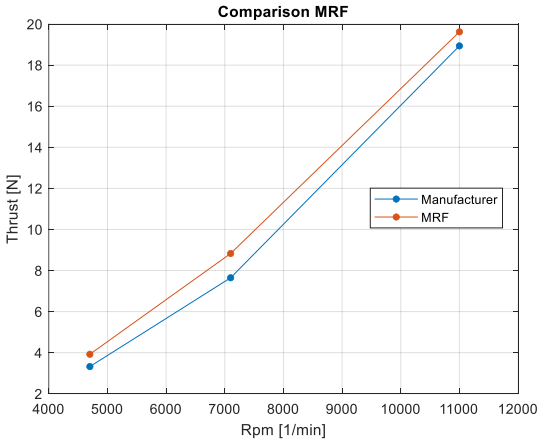

Figure 36: Comparison MRF

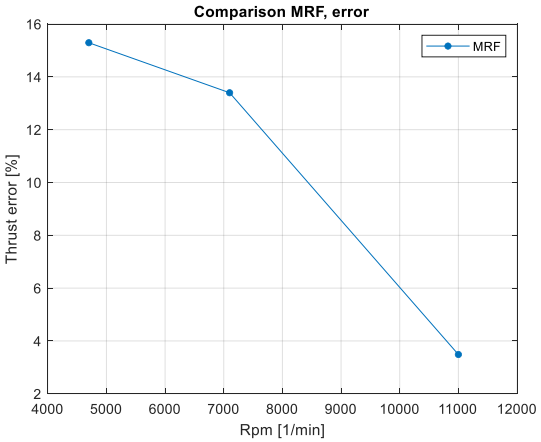

Figure 37: Comparison MRF, error

Table 8: Comparison MRF

n [rpm]	Thrust manufacturer [N]	Thrust MRF [N]
4700	3,92	3,32
7100	8,83	7,65
11000	19,6	18,9

Propeller characteristics

To analyze the propeller characteristics of the MRF for a β equal to zero degrees, the same simulation operation from the virtual disk is used.

Therefore a few conclusions can be made. The efficiency and the thrust coefficient have the expected behavior in function of the advance ratio like the literature teaches. For the power coefficient that failed the virtual disk, better results are accomplished.

For low advance ratios, the power coefficient pretty much stays constant. The power coefficient rises slightly in function of the advance ratio at low advance ratios. However this slight increase is negligible due to the small absolute percentual error of 0,70% between the first value of power coefficient at the lowest advance ratio and the maximum power coefficient.

When the rotational speed is increased, the maximum thrust coefficient, maximum power coefficient and maximum efficiency rises. The position of the maximum efficiency shifts slightly to a higher advance ratio when the rotational speed is increased.

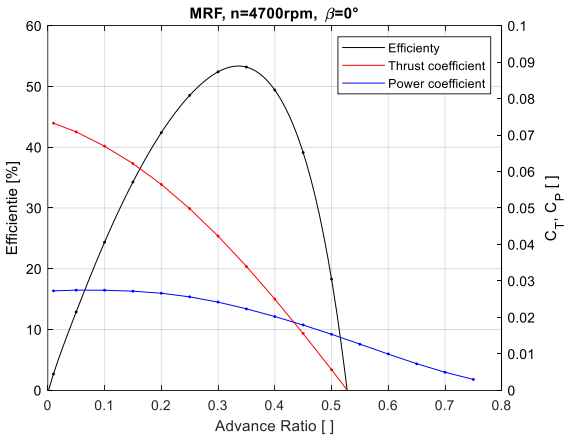

Figure 38: MRF characteristics 4700rpm

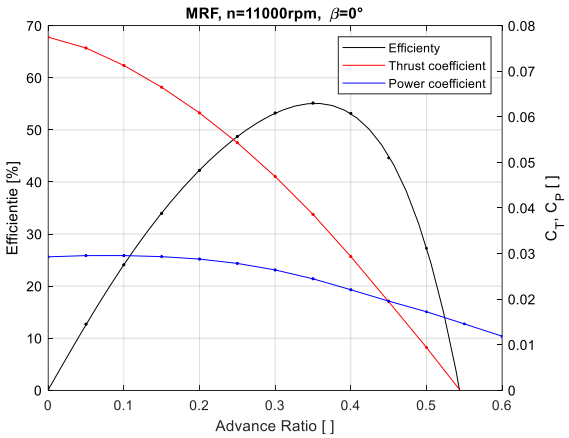

Figure 39: MRF characteristics 11000rpm

5.4 MRF in oblique flow

The MRF in oblique flow uses again the same conventions, where theta is the radial position and beta the angle of oblique flow.

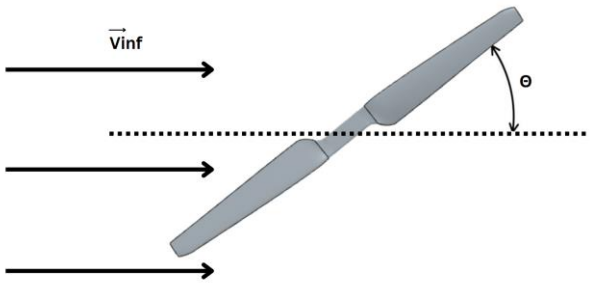

Figure 40: Radial position theta

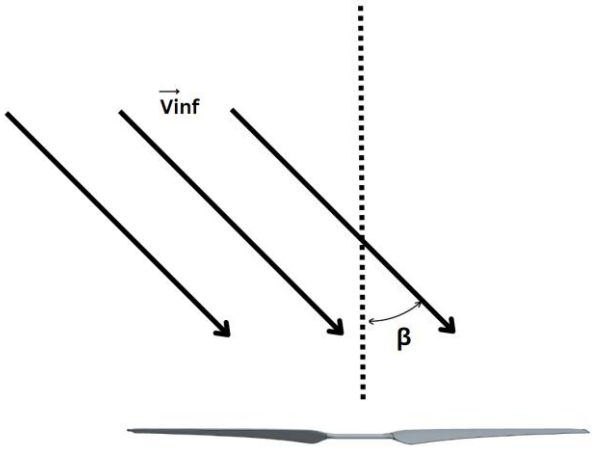

Figure 41: Angle beta, oblique flow

Propeller characteristics

First of all the performance of the propeller is analyzed in function of the oblique flow angle. Regarding the characterization is done for the same values of J like the pure vertical flow, the advance ratio normal to the propeller will be different, this value will drop when the oblique flow becomes more horizontal. Invisible on the plots, but regarding the regressions connecting the measurements of the efficiency, the efficiency drops slightly in function of the angle beta.

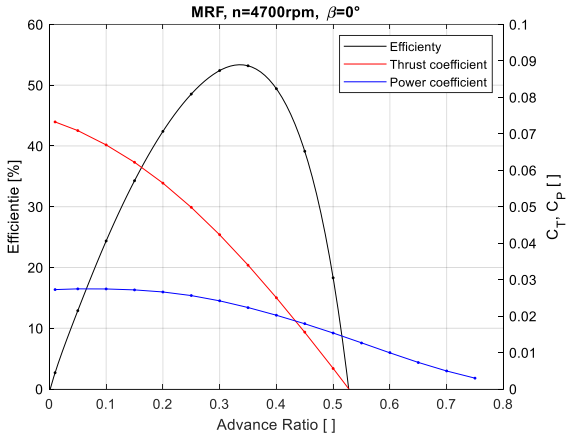

Figure 42: Characteristics, β=0°

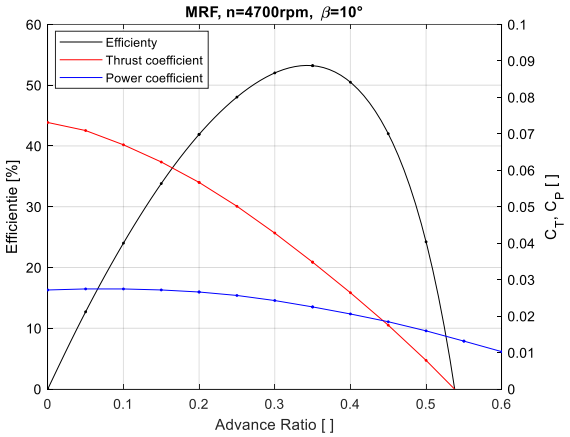

Figure 43: Characteristics, β=10°

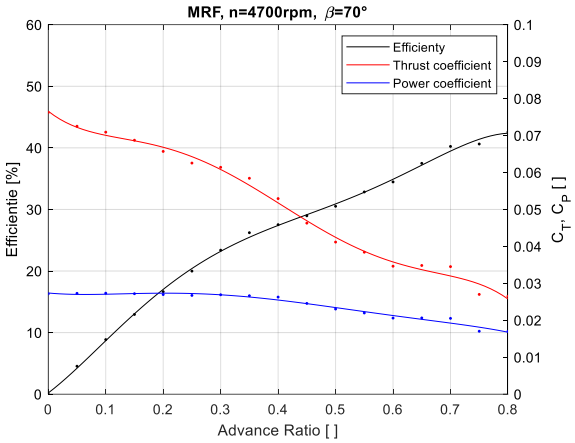

Figure 44: Characteristics, β=70°

How more oblique the flow becomes, how more the curves get stretched along the horizontal where the advance ratio is shown. This is because the propeller characteristics mainly rely on the normal advance ratio. When compared the vertical flow and the oblique flow for an angle of 70 degrees for the same normal advance ratio. For example, when we select for an oblique flow of degrees an advance ratio of 0.585, the normal advance ratio is equal to 0.4, the next following results can be compared.

Table 9: Comparison oblique flow MRF

β [°]	J [ ]	Jn [ ]	C_T [ ]	C_p [ ]	η [%]
0	0,400	0,400	0,0250	0,0202	49,4
70	0,575	0,400	0,0392	0,0219	35,7

Oblique flow increases the thrust and power for a certain advance ratio, but at the cost of efficiency.

Blades thrust

To compare the results of the different types of interfaces are compared. The average of the mixing-plane interface can be confirmed by the total thrust of the internal interface.

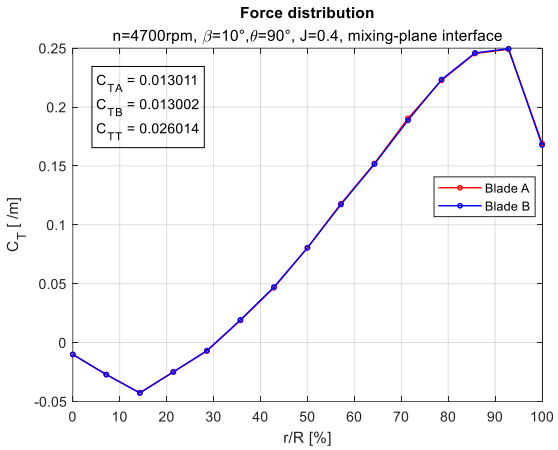

Figure 45: Force distribution MRF, β=10°, θ=90°

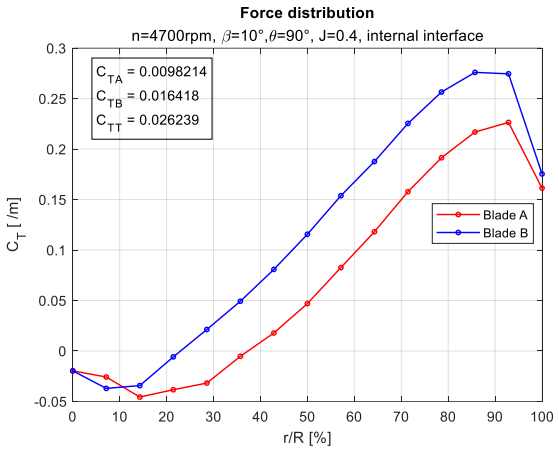

Figure 46: Force distribution MRF, β=10°, θ=90°

Despite the averaging in the mixing-plane interface, there is still a minor difference in thrust between blade A and blade B, however this negligible due to the small absolute difference of 0,0692%. The use of the internal interface results in an equal total thrust coefficient, compared to the mixing-plane interface there is a small absolute difference 0,861% witch can be neglected as well.

When analyzing figure 46 shown above, there is a strange situation happening. As explained before in chapter 4.9.2, the advancing blade should have a higher value for the trust and velocity compared to the retreating blade.

Now in this situation. A high flow velocity, a lower pressure at the suction side of the advancing blade and thus a higher lift coefficient is expected. However the pressure on the suction side and velocity is not as expected.

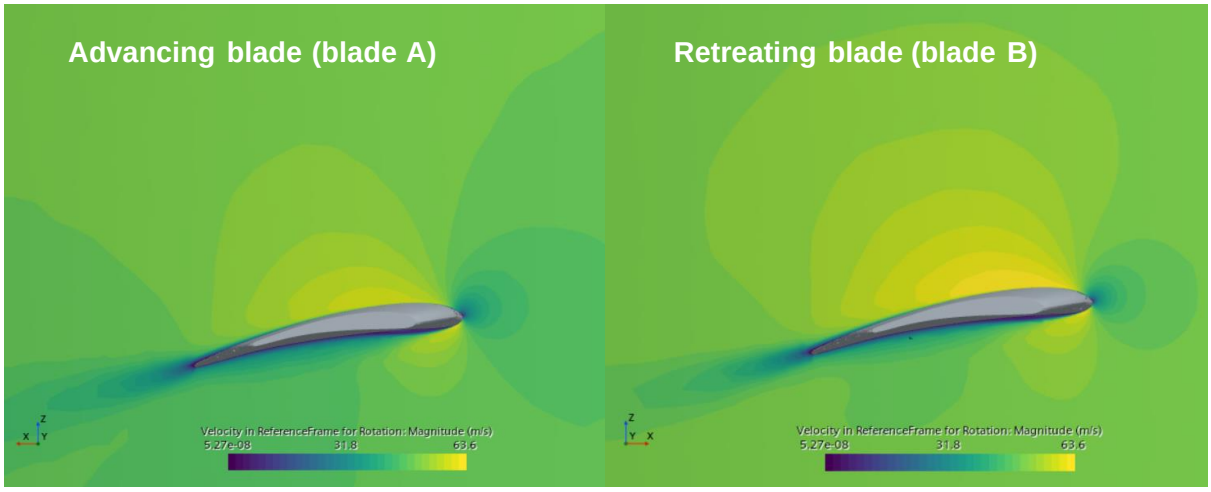

Figure 47: Velocity field, β=10°, θ=90°

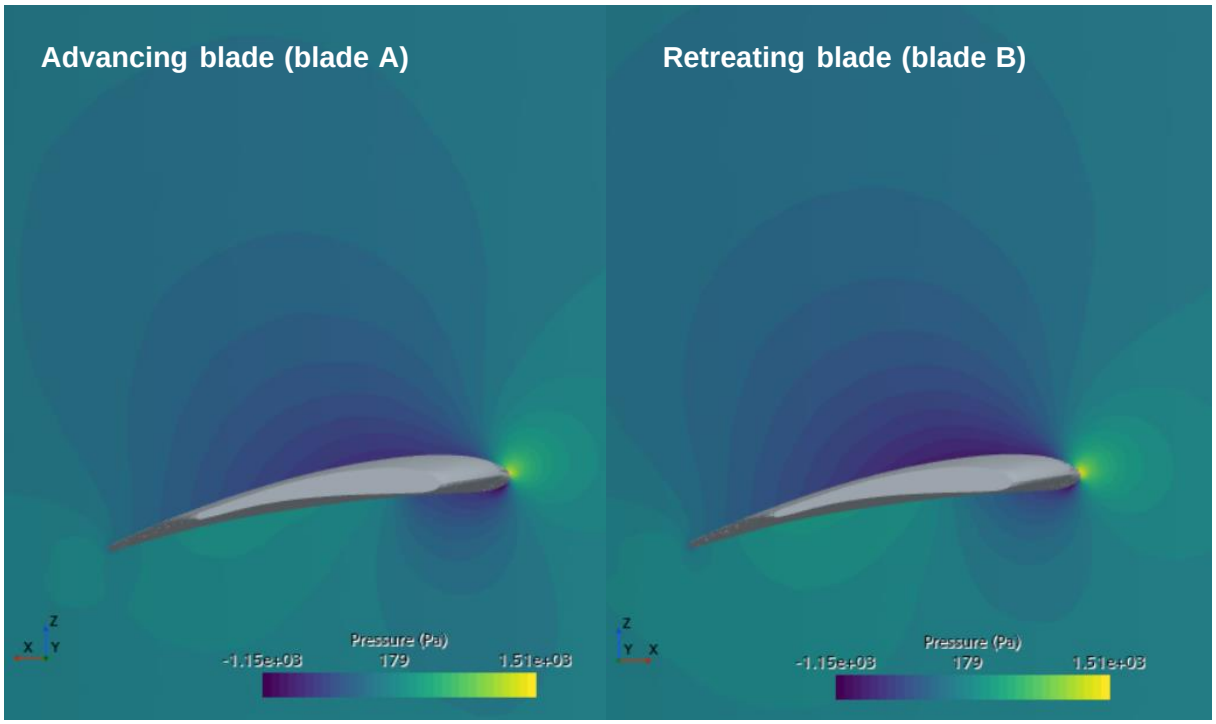

Figure 48: Pressure field, β=10°, θ=90°

When the propeller is rotated back to its original position where θ is zero degrees, we get the following results for force distribution, velocity, and pressure, shown in the figures below. As expected, the thrust of both blades should not be very different because the blade velocity's should be equal. However, blade A has the highest thrust, and blade B has the lowest. In this case, blade A is the downstream blade, and blade B is the upstream blade. The results of the graph match with the velocity and pressure around the blades: blade A has a higher velocity and lower pressure on the suction side, leading to higher thrust.

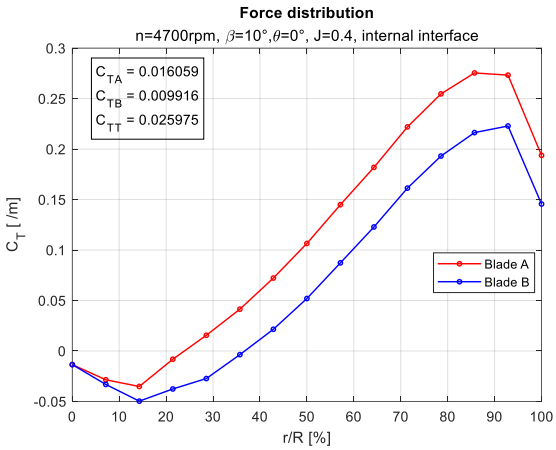

Figure 49: Force distribution MRF, β=10°, θ=0°

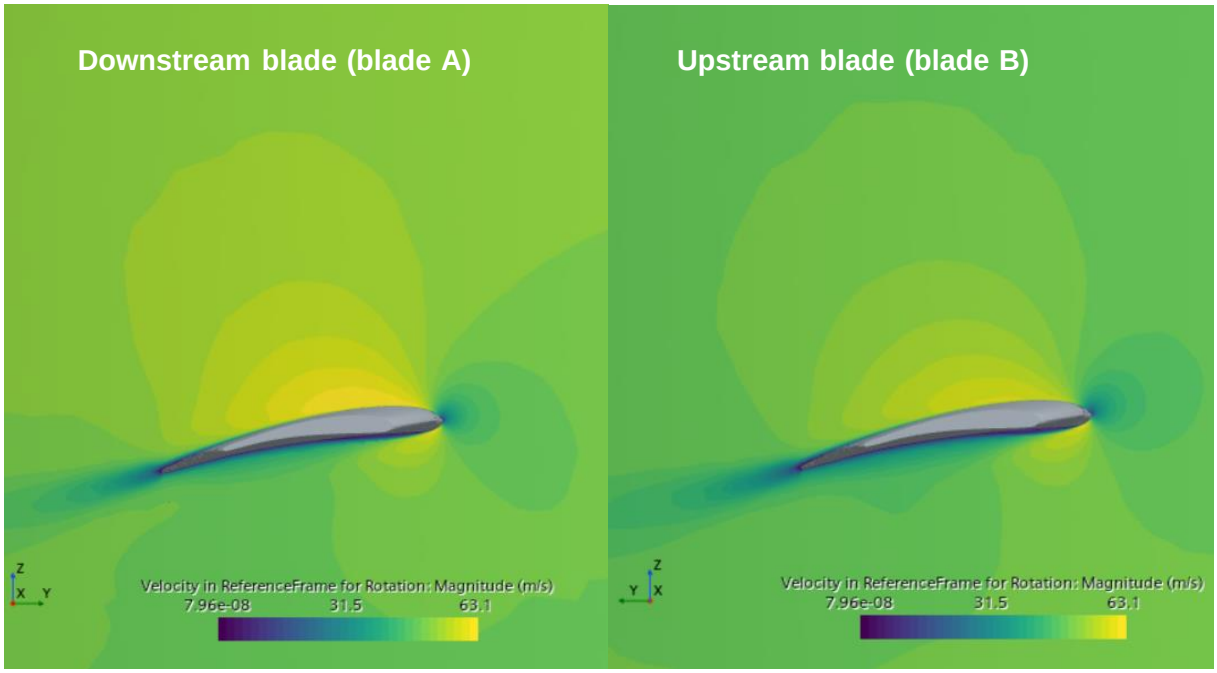

Figure 50: Velocity field, β=10°, θ=0°

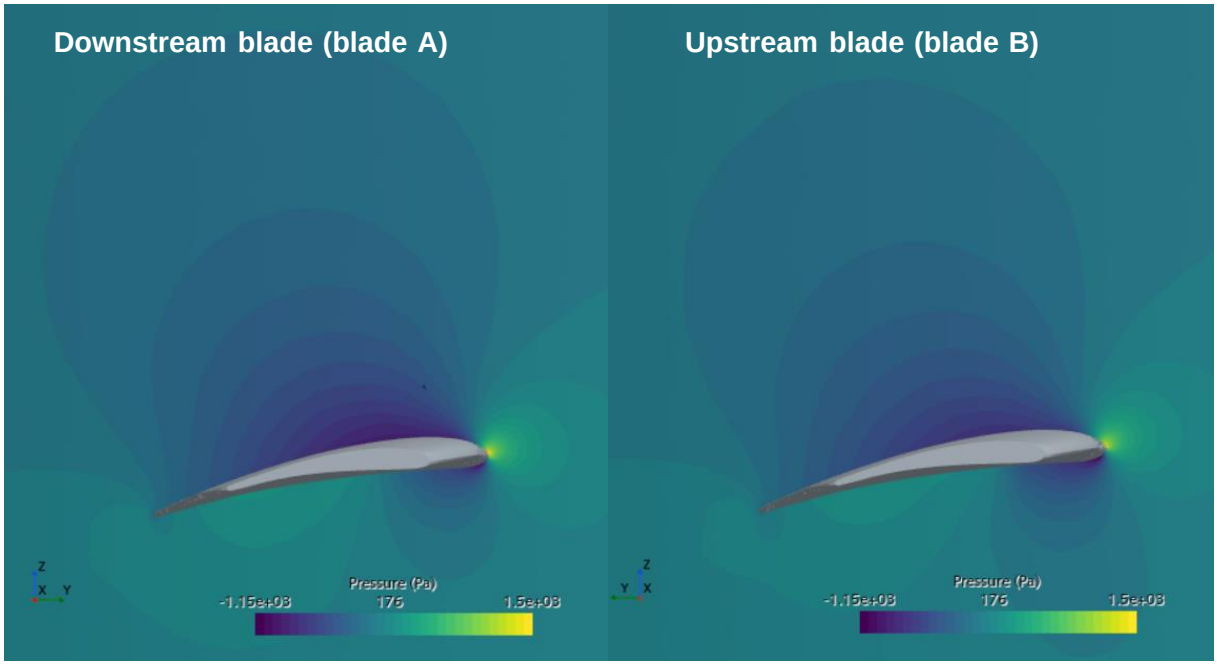

Figure 51: Pressure field, β=10°, θ=0°

We can conclude that the thrust values for each blade make sense when looking at the velocity and pressure around the blade. However, these values don't make sense when compared to the radial position of the blade (given by θ). Since we want to study how the propeller behaves in oblique flow, we can't use this method anymore. Instead, we will switch to a transient simulation. This will let us examine what happens around the blades based on their radial position.

5.5 RBM

The conventions of the RBM are the same as the MRF, where theta is the radial position and beta the angle of oblique flow, shown below.

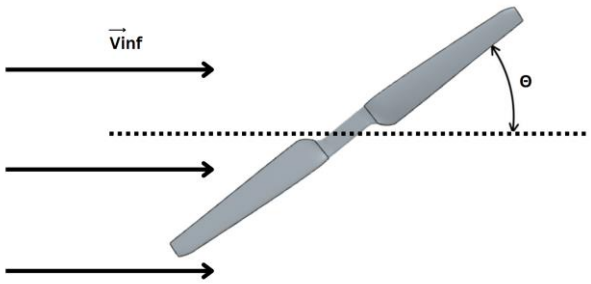

Figure 52: Radial position theta

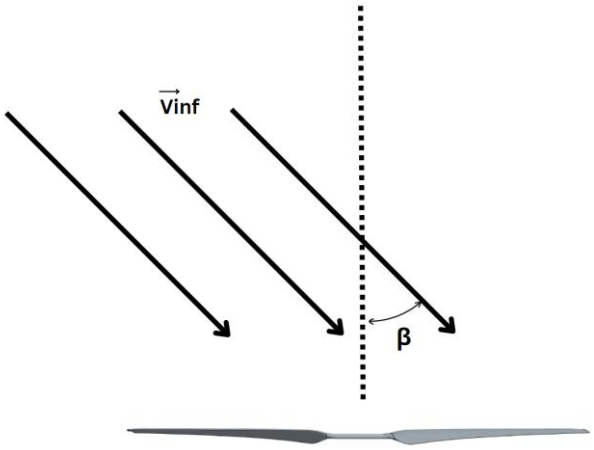

Figure 53: Angle beta, oblique flow

Blade thrust for low angles

Blade A, shown by the dotted lines, clearly has the highest thrust when moving forward. However, there's a slight delay in reaching its maximum thrust, which is expected at a 90-degree position.

As the advance ratio increases, the thrust amplitude of both blades decreases. The same happens when the angle of the oblique flow increases. This is because blade thrust depends on the normal advance ratio; the smaller this ratio, the higher the thrust. In oblique flow, the normal component of the advance ratio decreases as the angle β increases, which leads to a decrease in thrust.

For an advance ratio of 0.8, the results seem unreliable due to irregular patterns.

When the oblique flow angle is zero degrees, the thrust of both blades should be the same and constant. This is true for advance ratios of 0.2 and 0.4, with only minor errors. However, for an advance ratio of 0.8, the thrust development becomes unreliable even at low oblique flow angles.

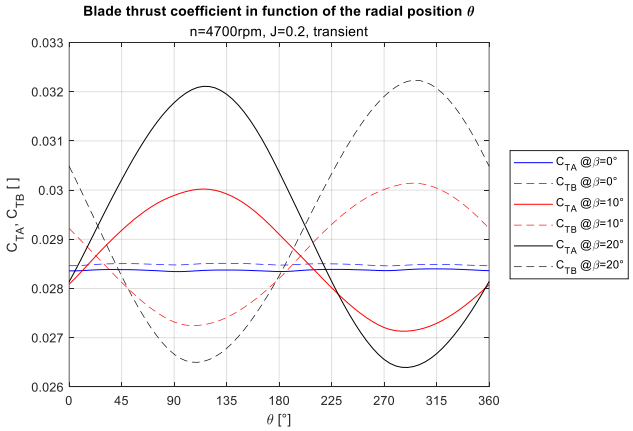

Figure 55: Blade thrust, J=0.2

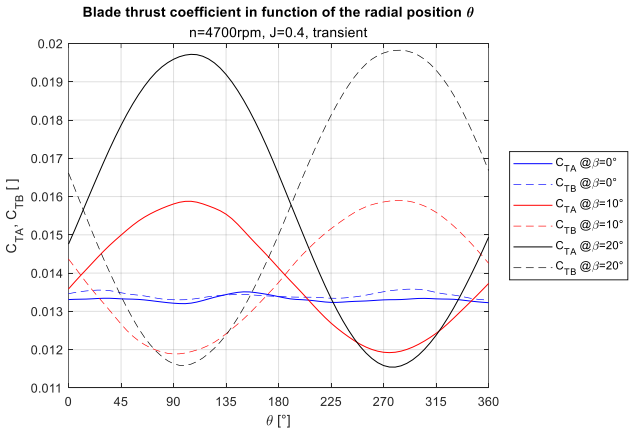

Figure 54: Blade thrust, J=0.4

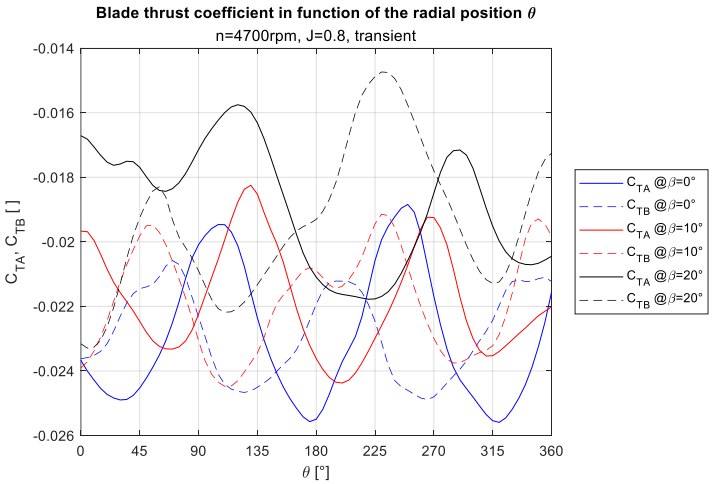

Figure 56: Blade thrust, J=0.8

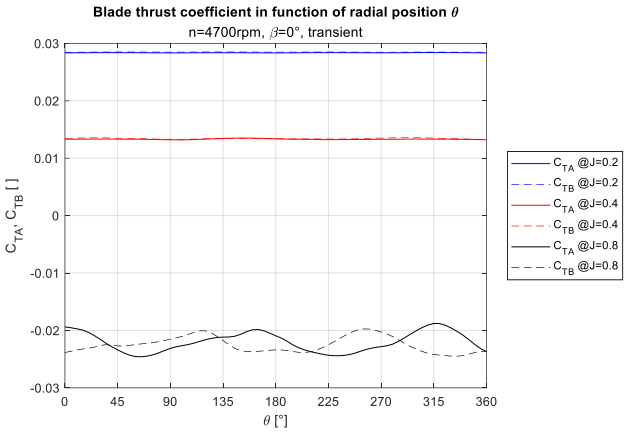

Figure 58: Blade thrust, β=0°

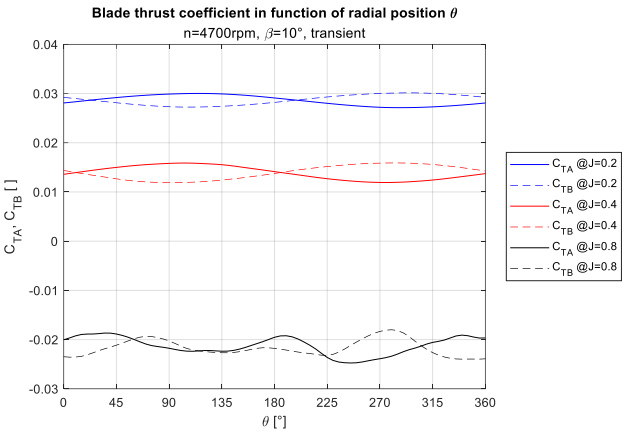

Figure 57: Blade thrust, β=10°

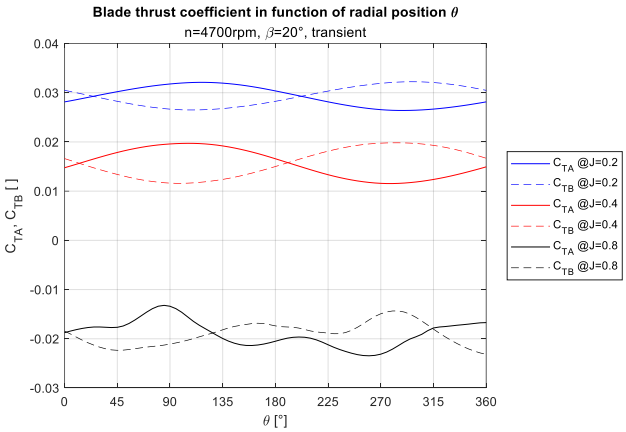

Figure 59: Blade thrust, β=10°

Total thrust for low angles

For the total thrust at low angles of oblique flow, similar observations can be made as for the thrust of each blade. When the advance ratio decreases or the angle β increases, the total thrust of the propeller increases. However, for an advance ratio of 0.8, the results are irregular.

The total thrust remains constant relative to the radial position, aside from minor fluctuations.

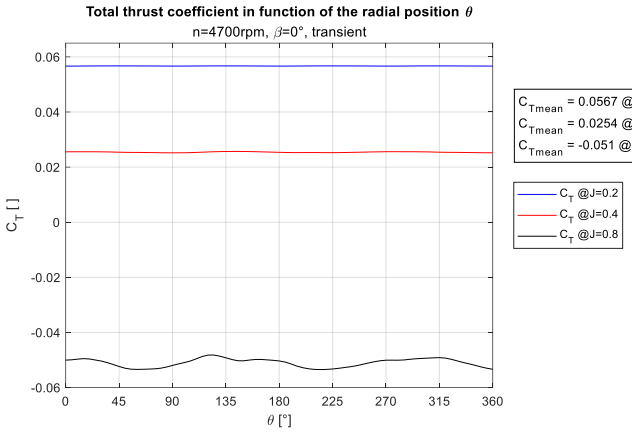

Figure 60: Total thrust, β=0°

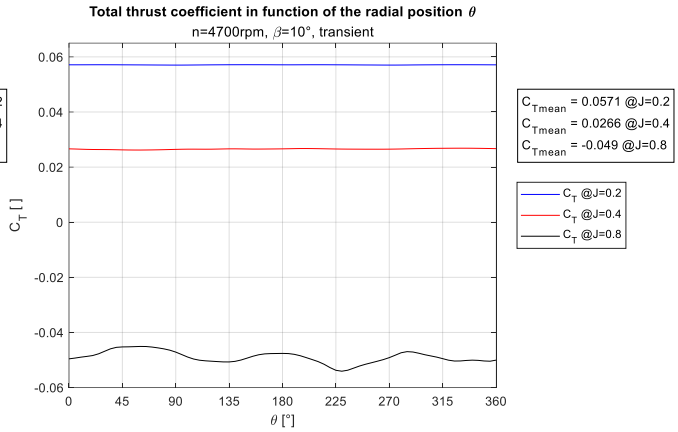

Figure 61: Total thrust, β=10°

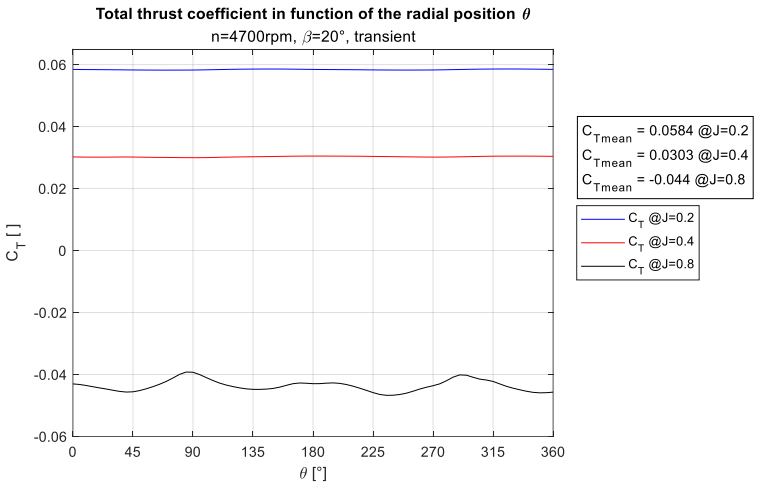

Figure 62: Total thrust, β=20°

Blade thrust for high angles

At high angles of oblique flow, the behavior of the blades in relation to the radial position of the propeller is similar to that at low angles of oblique flow. However, the radial position where blade A reaches its maximum thrust shifts, approximately doubling compared to the low angle of β.

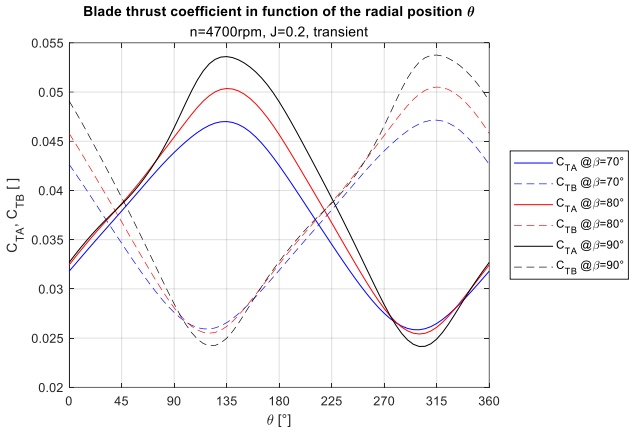

Figure 63: Blade thrust, J=0.2

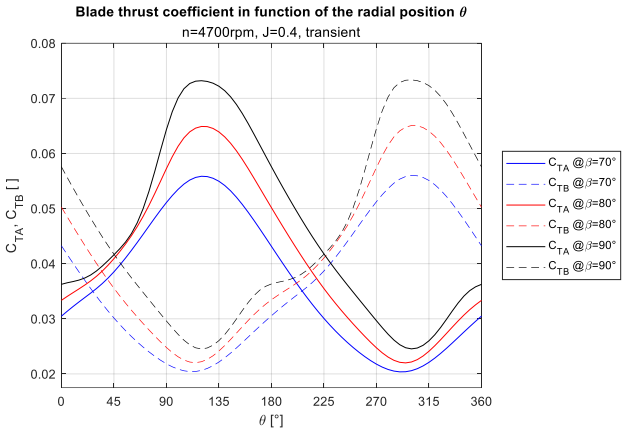

Figure 64: Blade thrust, J=0.4

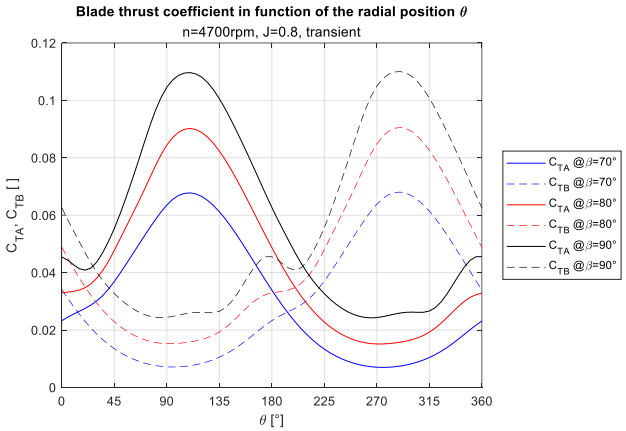

Figure 65: Blade thrust, J=0.8

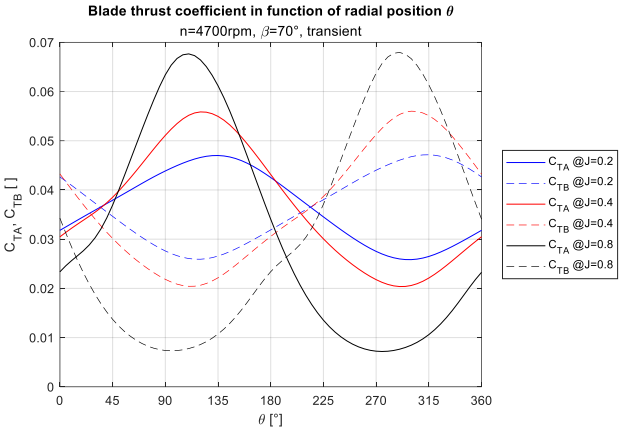

Figure 67: Blade thrust, β=70°

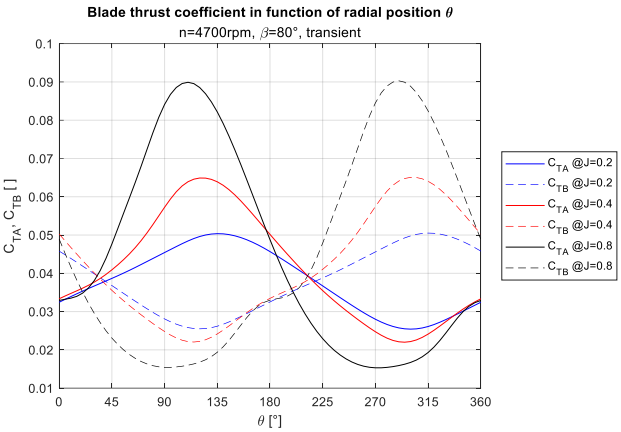

Figure 66: Blade thrust, β=80°

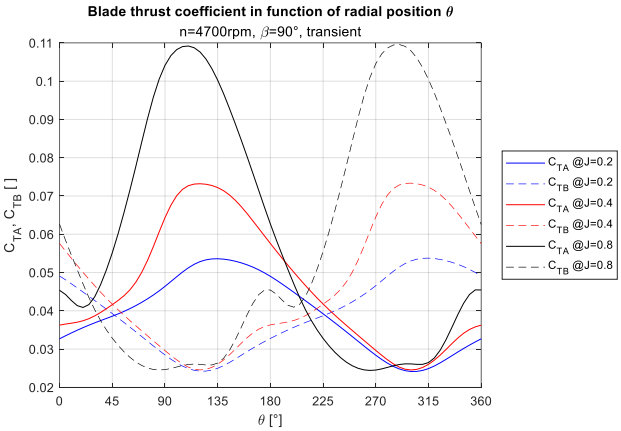

Figure 68: Blade thrust, β=90°

Total thrust for high angles

Compared to the results for low values of β, similar observations apply. However, the total thrust does not remain constant in the scenario described below. It is evident that periodic oscillations occur in the figures. These oscillations have a period of 180°, reflecting the symmetry of the propeller with two identical blades.

As the advance ratio decreases, the amplitude of the total thrust decreases, but the average thrust over one rotation increases. The peak of each period shifts to the right on the curve as the advance ratio decreases.

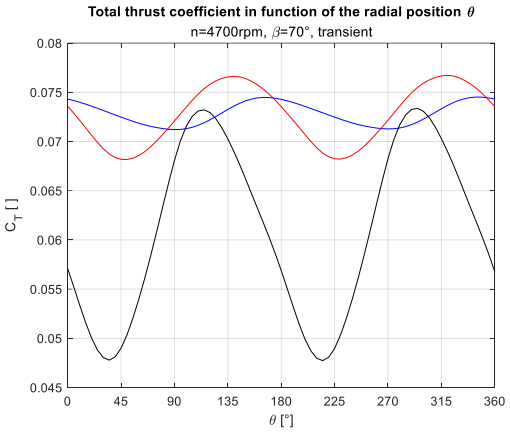

Figure 70: Total thrust, β=70°

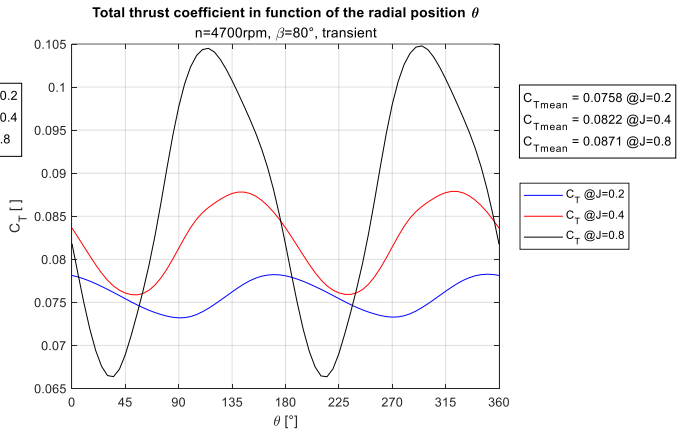

Figure 69: Total thrust, β=80°

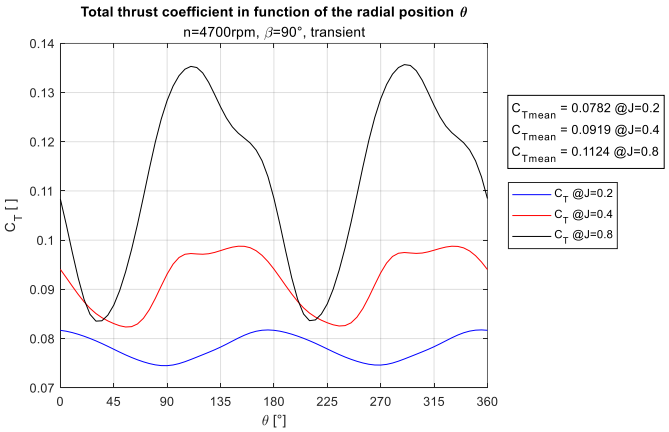

Figure 71: Total thrust, β=90°

Force distributions

On the figures below, the force distributions for three angles of β are shown (0°, 70° and 90°), each for three different advance ratios. It is clear that for vertical flight, the thrust of blade A is equal to the thrust of blade B. As mentioned earlier, for higher advance ratios, the thrust coefficients drops. The simulations for an advance ratio of 0.8 for a β of 0° can be ignored again due to incorrect results.

When the flow turns oblique, the thrust of both blades aren't equal anymore, the advancing blade has a higher thrust than the retreating blade which is clearly visible for the flow for a β of 70°.

In all cases the 'tip loss effect' is clearly visible. At around 95% of the blade, the thrust coefficient drops to almost 0.

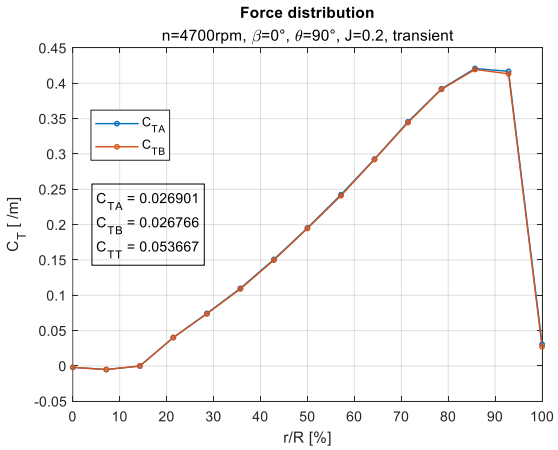

Figure 72: Force distribution β=0°, θ=90°, n=0.2

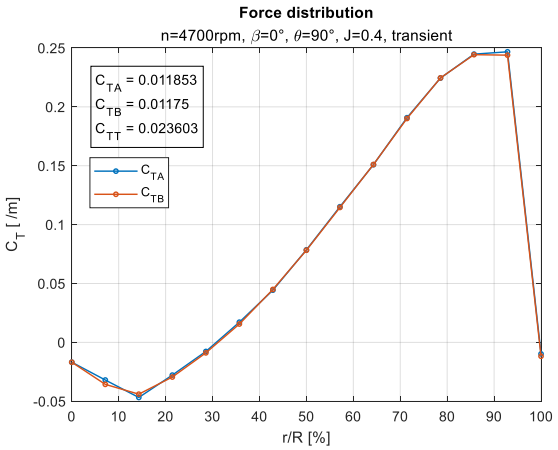

Figure 73: Force distribution β=0°, θ=90°, n =0.4

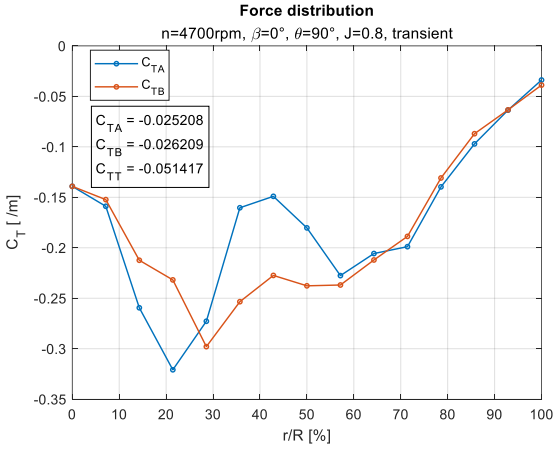

Figure 74: Force distribution β=0°, θ=90°, n=0.8

At high beta angles, the force distributions align with theoretical predictions. A clear distinction is observed between the advancing blade (blade A) and the retreating blade (blade B). The advancing blade shows a significantly higher total thrust. This thrust increases with the radius, corresponding to the increasing velocity difference between the two blades as the radius grows. Additionally, similar to vertical flow, the "tip loss effect" is noticeable at the ends of the blades.

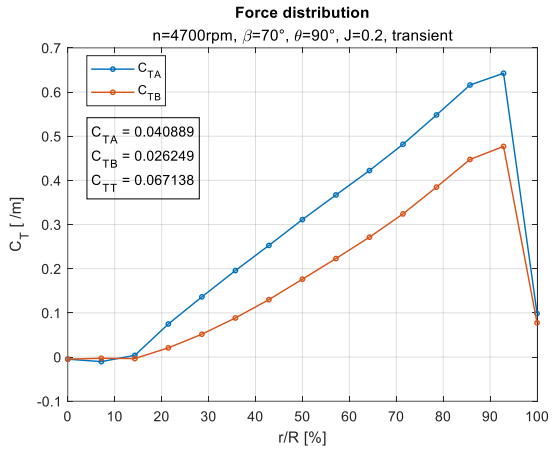

Figure 75: Force distribution β=70°, θ=90°, n=0.2

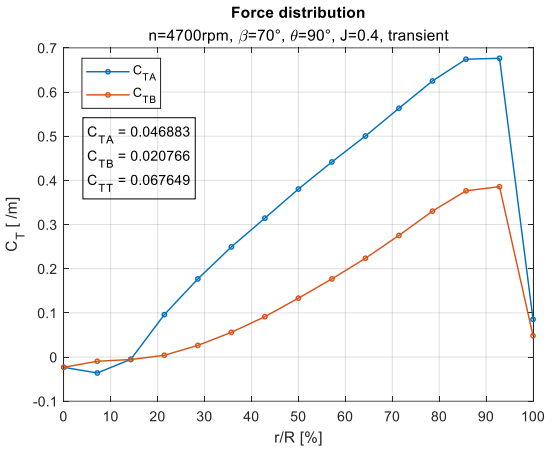

Figure 76: Force distribution β=70°, θ=90°, n=0.4

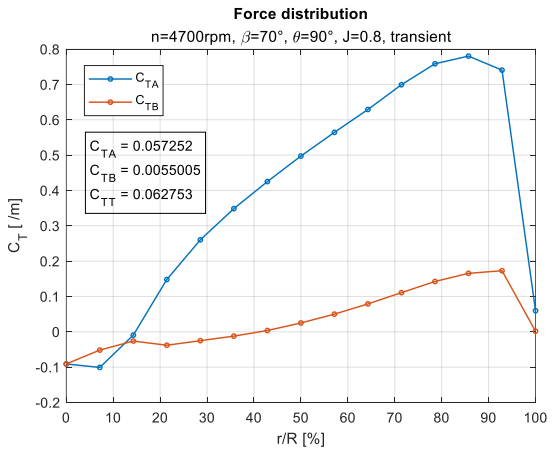

Figure 77: Force distribution β=70°, θ=90°, n=0.8

Pressure and velocity fields

The pressure and velocity fields confirm the earlier numerical results for a radial position of 90°. Blade A, the advancing blade shown on the left, has a noticeable higher velocity than blade B, the retreating blade. These velocities have influence on the pressure around the blades. Due to the higher velocity of blade A, a lower pressure on the suction side and higher pressure on the bottom side is noticed compared to Blade B, the retreating blade.

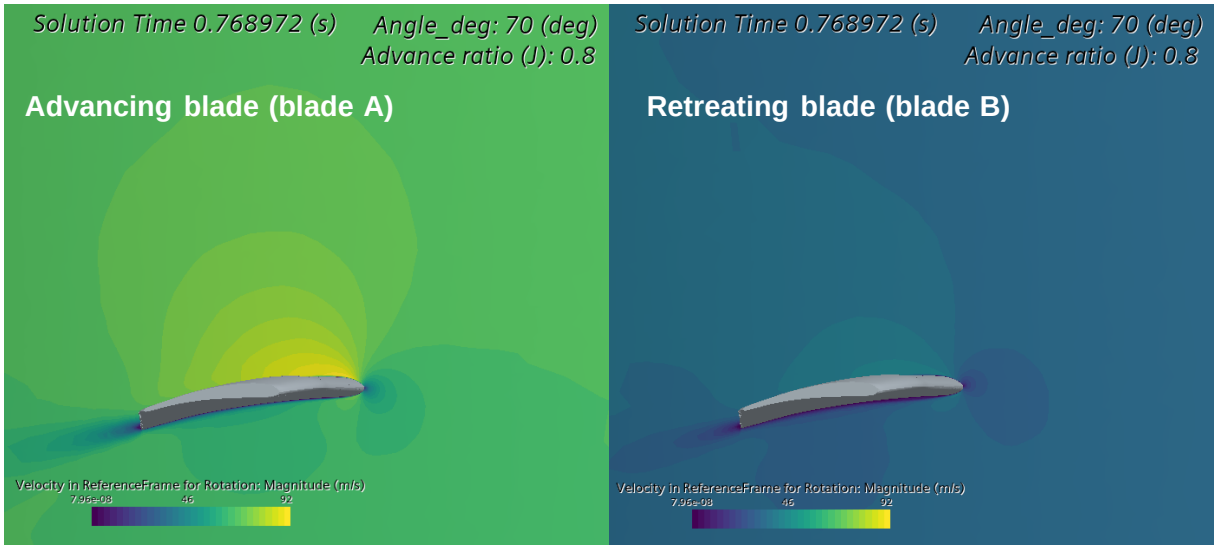

Figure 78: Velocity fields transient

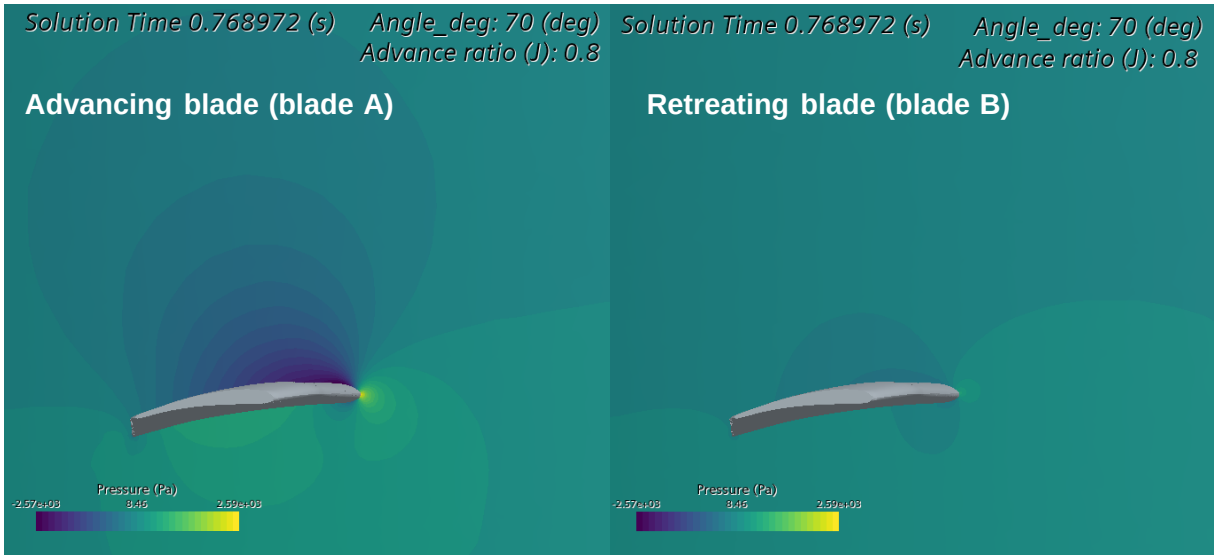

Figure 79: Pressure fields transient

5.5.1 Comparison with MRF

Even for the global results of the propeller, different results are obtained between the MRF and the RBM.

Table 10: MRF vs RBM

	MRF	**RMB**
C_T @J=0,4 ; β=0°	0,0250	0,0254
C_T @J=0,4 ; β=10°	0,0264	0,0266
C_T @J=0,4 ; β=70°	0,0529	0,0727

The difference in total thrust between the two methods, increases when the angle of oblique flow increases. Due to no manufacturer data, the correctness can't be obtained.

6 CONCLUSION AND FUTURE WORK

The findings of this research have provided significant insights into the behavior of propeller blades under various flow conditions. Specifically, the analysis of force distributions at high beta angles has shown a strong alignment with theoretical predictions, highlighting distinct differences between the advancing and retreating blades. However, it was found that some CFD models are not suitable for certain types of analysis.

The Virtual Disk model proves to be effective for simulating vertical flight and reducing simulation time, but it is not valid for analyzing oblique flow. For such cases, the MRF (Moving Reference Frame) model is a better choice, delivering reliable results for oblique flow conditions. However, when the focus is on studying the behavior of individual blades, transitioning to a transient simulation using Rigid Body Motion (RBM) is necessary. The RBM model effectively illustrates the behavior of propeller blades, though for numerical metrics like total thrust, the MRF model remains adequate.

In summary, the choice of the CFD model should be based on the specific requirements of the analysis, with the Virtual Disk model being suitable for vertical flight simulations, the MRF model for oblique flow conditions, and the RBM model for detailed blade behavior analysis.

General, the efficiency of a propeller rises in function of the rotational speed (in the rotational speed range that is used) and drops in function of the angle beta same as the total thrust and power. The advance ratio for maximum efficiency rises in function of the angle beta.

As future work, the further analyze of oblique flow could be done for the fuselage of the drone and for the full setup, the drone with the propellers.

7 BUDGET

As for the supervisor, the compensation received by PhD from UPV with teaching and research activities, in this case at CMT, working 40 hours per week is assumed to be €30.82/hour.

Description	Cost [€/h]	Duration [h]	Total [€]
PhD student	12,82	8	102,56
Supervisor	30,82	30	924,60

In projects like this, it is important to consider additional costs related to IT tools, such as hardware and software costs.

Description	Cost [€/month]	Duration [month]	Total [€]

STAR-CCM+	2797	4	6666
Laptop	23,33	4	93,33

The total cost of the project results in:

Total cost before VAT (21%): €7786,49

Total cost: €9421,65

8 DEVELOPMENT GOALS

SDG	High	Medium	Low	Not applicable
1. No poverty				x
2. Zero hunger				x
3. Good health and well-being				x
4. Quality education				x
5. Gender equality				x
6. Clean water and sanitation				x
7. Affordable and clean energy		x		
8. Decent work and economic growth			x	
9. Industry, innovation and infrastructure	x			

10. Reduced inequality				x
11. Sustainable cities and communities	x			
12. Responsible consumption and production			x	
13. Climate action	x			
14. Life below water				x
15. Life on land		x		
16. Peace, justice, and strong institutions				x
17. Partnerships for the goals		x		

9 BIBLIOGRAFIE

MS1101-2PCS/PAIR_Polymer Straight_Polymer_Propellers_UAV Power_T-MOTOR Official Store - UAV Power System, Robot Power System, Model Power System. (z.d.). https://store.tmotor.com/product/ms1101-polymer-straight.html

Yu, D., Wang, L., Liu, H., & Cui, M. (2023). Influence of Load Conditions on the Propeller Wake Evolution. *Journal Of Marine Science And Engineering*, *11*(9), 1674. https://doi.org/10.3390/jmse11091674

Bardina, J. E., Huang, P. G., & Coakley, T. J. (1997, April 1). *Turbulence modeling validation, testing, and development*. NASA Technical Reports Server (NTRS). https://ntrs.nasa.gov/citations/19970017828

Simcenter STAR-CCM+ CFD software. (n.d.). Siemens Digital Industries Software. https://plm.sw.siemens.com/en-US/simcenter/fluids-thermal-simulation/star-ccm/

Flow over immersed bodies. (2017, 3 juli). Ppt Video Online Download. https://slideplayer.com/slide/4945831/

Bekaert, Ing. (z.d.). *Aerodynamica II - Computational Fluid Dynamics* [Presentatieslides].

Mullen Brendan. (z.d.). *Assessing the performance characteristics of a quad-copter unmanned aerial vehicle using computational fluid dynamics*. UPV.

Liu, Z., Liu, P. Q., Qu, Q., & Hu, T. (2016). Effect of Advance Ratio and Blade Planform on the Propeller Performance of a High Altitude Airship. *Journal Of Applied Fluid Mechanics.*, *9*(6), 2993–3000. https://doi.org/10.29252/jafm.09.06.25203

Miao, W., Liu, Q., Xu, Z., Yue, M., Li, C., & Zhang, W. (2022). A comprehensive analysis of blade tip for vertical axis wind turbine: Aerodynamics and the tip loss effect. *Energy Conversion And Management*, *253*, 115140. https://doi.org/10.1016/j.enconman.2021.115140

Johan. (2022, 26 augustus). How to setup Rigid Body Motion (RBM) and Moving Reference Frame (MRF) simulations in Simcenter STAR-CCM+ - VOLUPE Software. *VOLUPE Software*. https://volupe.se/how-to-setup-rigid-body-motion-rbm-and-moving-reference-frame-mrf-simulations-in-simcenter-star-ccm/

Fraser-Mitchell, A. (2012). Fundamentals of Aerodynamics — Fifth edition, J. D. Anderson, McGraw-Hill, Shoppenhangers Road, Maidenhead, Berkshire, SL6 2QL, UK. 2011. 1098pp. Illustrated. £47.99. ISBN 978-007-128908-5. ˜ *The œAeronautical Journal/Aeronautical Journal*, *116*(1176), 222–223. https://doi.org/10.1017/s000192400000676x

Day, A. M. K. D. O. A. V. (2000). Effects of Bend–Twist Coupling on Composite Propeller Performance. *Mechanics Of Composite Materials And Structures*, *7*(4), 383–401. https://doi.org/10.1080/10759410050201717

Ansys. (2024) https://www.ansys.com/simulation-topics/what-is-computational-fluid-dynamics

10 ATTACHMENTS

10.1 Twist and chord

r [m]	r/R [ ]	c [m]	c/R [ ]	AoA [rad]	AoA [°]
0,0012768	0,00912	0,012	0,085714286	0	0
0,014	0,1	0,012	0,085714286	0	0
0,021	0,15	0,017	0,121428571	0,174532925199433	0,174532925
0,028	0,2	0,024	0,171428571	0,337860836601062	0,337860837
0,035	0,25	0,024	0,171428571	0,315415902420415	0,315415902
0,042	0,3	0,0234	0,167142857	0,293232767627567	0,293232768
0,049	0,35	0,0228	0,162857143	0,270526034059121	0,270526034
0,056	0,4	0,0221	0,157857143	0,250734000341505	0,250734
0,063	0,45	0,0214	0,152857143	0,23460017673607	0,234600177
0,07	0,5	0,0207	0,147857143	0,219579873193407	0,219579873
0,077	0,55	0,0199	0,142142857	0,208793738416082	0,208793738
0,084	0,6	0,0192	0,137142857	0,196175007924163	0,196175008
0,091	0,65	0,0185	0,132142857	0,186034644970076	0,186034645
0,098	0,7	0,0178	0,127142857	0,179739242358132	0,179739242
0,105	0,75	0,017	0,121428571	0,173189021675397	0,173189022
0,112	0,8	0,0163	0,116428571	0,163991136517387	0,163991137
0,119	0,85	0,0156	0,111428571	0,159400920584642	0,159400921
0,126	0,9	0,0148	0,105714286	0,148806772025037	0,148806772
0,133	0,95	0,014	0,1	0,147375602038401	0,147375602

10.2 BEM

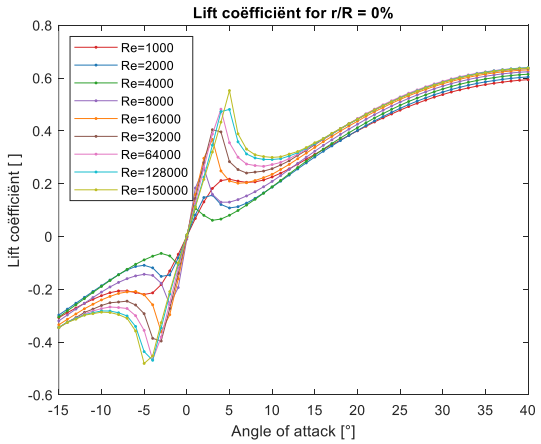
Lift coëfficiënt for r/R = 0%
Lift coëfficiënt [ ]
Angle of attack [°]
Re=1000
Re=2000
Re=4000
Re=8000
Re=16000
Re=32000
Re=64000
Re=128000
Re=150000

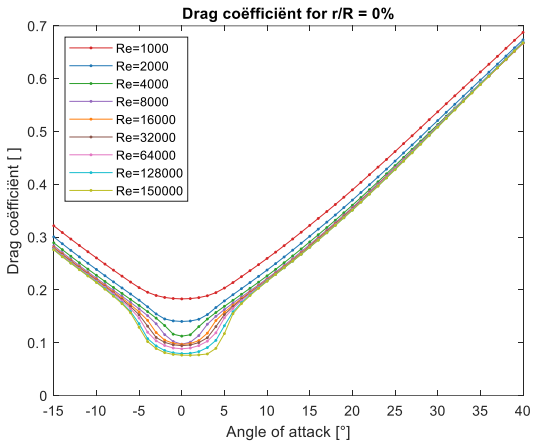
Drag coëfficiënt for r/R = 0%
Drag coëfficiënt [ ]
Angle of attack [°]
Re=1000
Re=2000
Re=4000
Re=8000
Re=16000
Re=32000
Re=64000
Re=128000
Re=150000

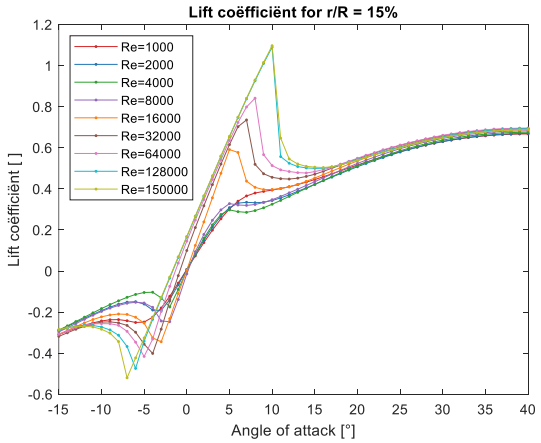
Lift coëfficiënt for r/R = 15%
Lift coëfficiënt [ ]
Angle of attack [°]
Re=1000
Re=2000
Re=4000
Re=8000
Re=16000
Re=32000
Re=64000
Re=128000
Re=150000

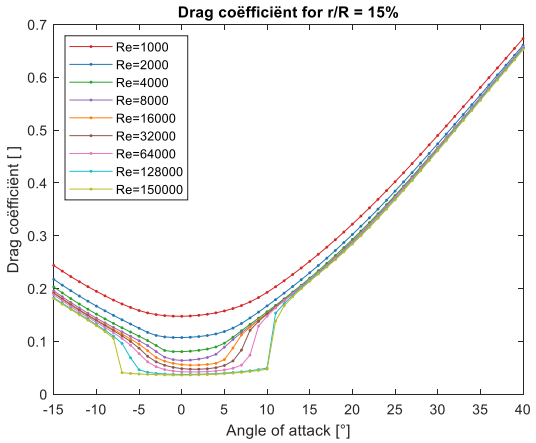
Drag coëfficiënt for r/R = 15%
Drag coëfficiënt [ ]
Angle of attack [°]
Re=1000
Re=2000
Re=4000
Re=8000
Re=16000
Re=32000
Re=64000
Re=128000
Re=150000

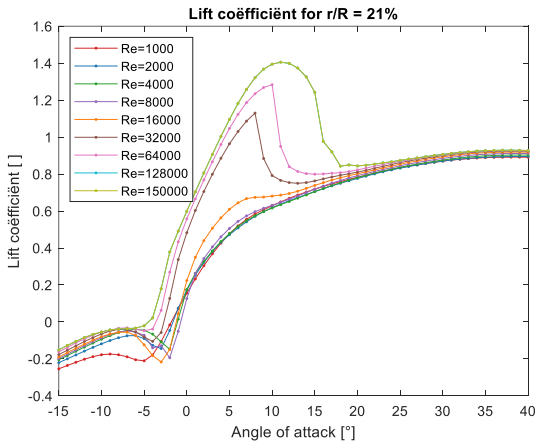
Lift coëfficiënt for r/R = 21%
Lift coëfficiënt [ ]
Angle of attack [°]
Re=1000
Re=2000
Re=4000
Re=8000
Re=16000
Re=32000
Re=64000
Re=128000
Re=150000

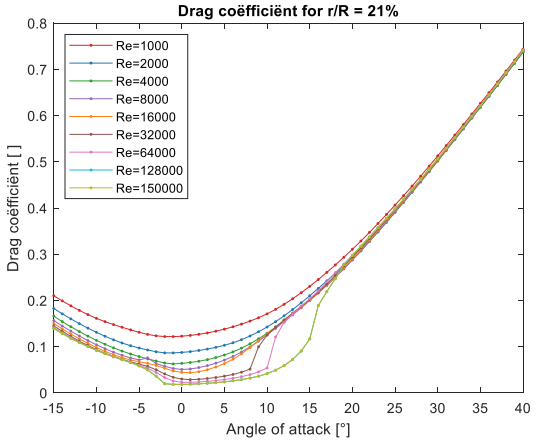
Drag coëfficiënt for r/R = 21%
Drag coëfficiënt [ ]
Angle of attack [°]
Re=1000
Re=2000
Re=4000
Re=8000
Re=16000
Re=32000
Re=64000
Re=128000
Re=150000

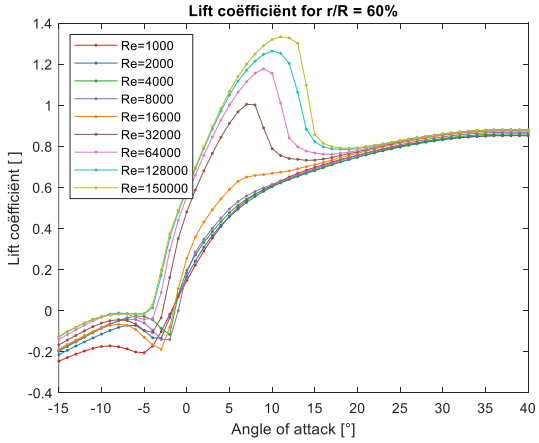
Lift coëfficiënt for r/R = 60%
Lift coëfficiënt [ ]
Angle of attack [°]
Re=1000
Re=2000
Re=4000
Re=8000
Re=16000
Re=32000
Re=64000
Re=128000
Re=150000

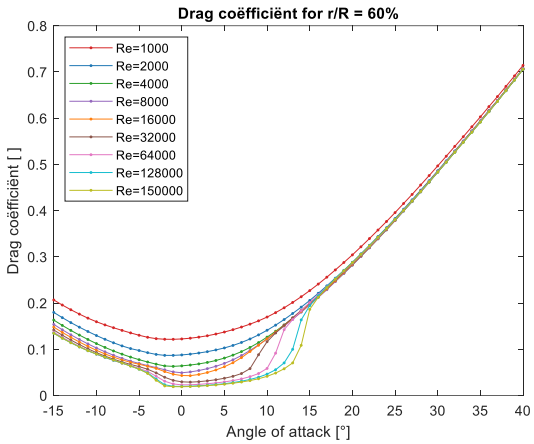
Drag coëfficiënt for r/R = 60%
Drag coëfficiënt [ ]
Angle of attack [°]
Re=1000
Re=2000
Re=4000
Re=8000
Re=16000
Re=32000
Re=64000
Re=128000
Re=150000

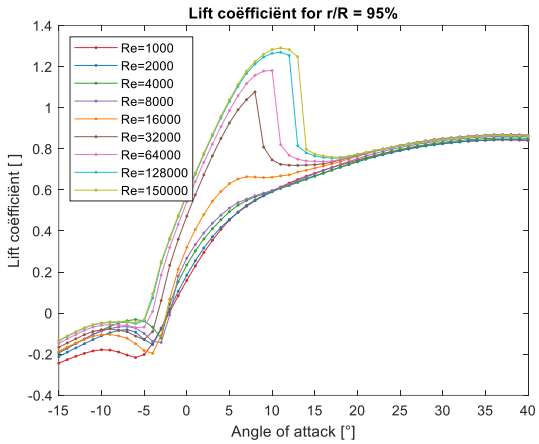
Lift coëfficiënt for r/R = 95%
Lift coëfficiënt [ ]
Angle of attack [°]
Re=1000
Re=2000
Re=4000
Re=8000
Re=16000
Re=32000
Re=64000
Re=128000
Re=150000

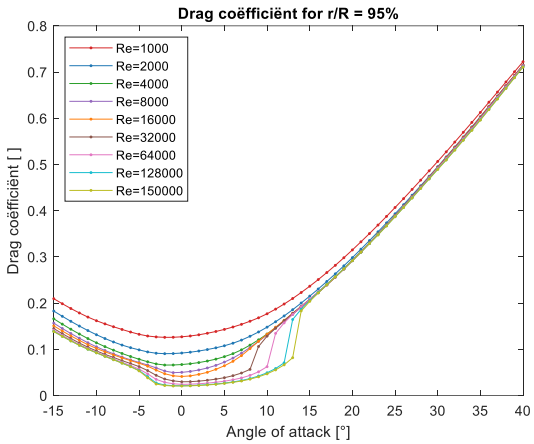
Drag coëfficiënt for r/R = 95%
Drag coëfficiënt [ ]
Angle of attack [°]
Re=1000
Re=2000
Re=4000
Re=8000
Re=16000
Re=32000
Re=64000
Re=128000
Re=150000

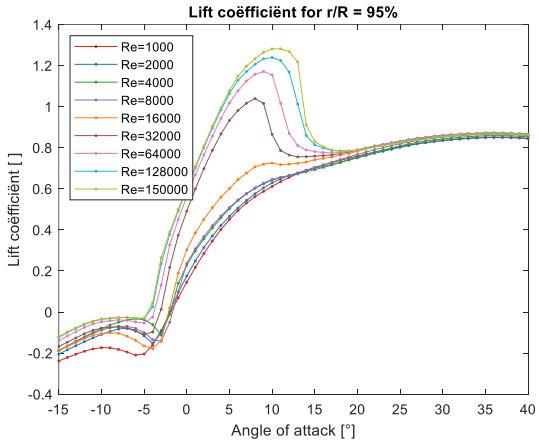
Lift coëfficiënt for r/R = 95%
Lift coëfficiënt [ ]
Angle of attack [°]
Re=1000
Re=2000
Re=4000
Re=8000
Re=16000
Re=32000
Re=64000
Re=128000
Re=150000

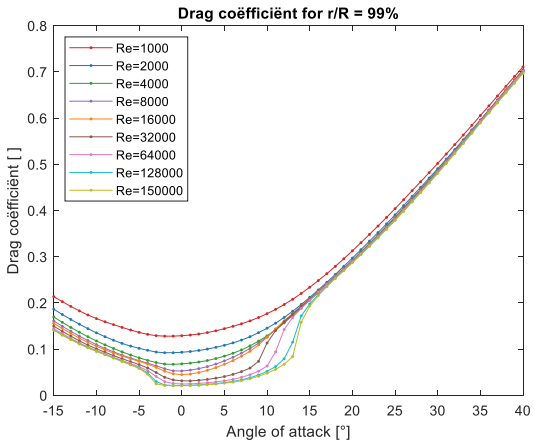
Drag coëfficiënt for r/R = 99%
Drag coëfficiënt [ ]
Angle of attack [°]
Re=1000
Re=2000
Re=4000
Re=8000
Re=16000
Re=32000
Re=64000
Re=128000
Re=150000

Clean Mobility & Thermofluids
UNIVERSITAT POLITÈCNICA DE VALÈNCIA

CAMINO DE VERA S/N 46022 VALENCIA. SPAIN
Tel: +34 96 387 76 50
E-mail: cmt@mot.upv.es